

Multi-metal porous crystalline materials for electrocatalysis applications

Ming Yue , Yi-Rong Wang , Jia-Yong Weng , Jia-Li Zhang ,
Da-Yu Chi , Mingjin Shi , Xiao-Gang Hu , Yifa Chen , Shun-Li Li ,
Ya-Qian Lan

PII: S1001-8417(24)00568-0
DOI: <https://doi.org/10.1016/j.cclet.2024.110049>
Reference: CCLET 110049



To appear in: *Chinese Chemical Letters*

Received date: 7 February 2024
Revised date: 4 May 2024
Accepted date: 24 May 2024

Please cite this article as: Ming Yue , Yi-Rong Wang , Jia-Yong Weng , Jia-Li Zhang , Da-Yu Chi , Mingjin Shi , Xiao-Gang Hu , Yifa Chen , Shun-Li Li , Ya-Qian Lan , Multi-metal porous crystalline materials for electrocatalysis applications, *Chinese Chemical Letters* (2024), doi: <https://doi.org/10.1016/j.cclet.2024.110049>

This is a PDF file of an article that has undergone enhancements after acceptance, such as the addition of a cover page and metadata, and formatting for readability, but it is not yet the definitive version of record. This version will undergo additional copyediting, typesetting and review before it is published in its final form, but we are providing this version to give early visibility of the article. Please note that, during the production process, errors may be discovered which could affect the content, and all legal disclaimers that apply to the journal pertain.

© 2024 Published by Elsevier B.V. on behalf of Chinese Chemical Society and Institute of Materia Medica, Chinese Academy of Medical Sciences.

Multi-metal porous crystalline materials for electrocatalysis applications

Ming Yue, Yi-Rong Wang*, Jia-Yong Weng, Jia-Li Zhang, Da-Yu Chi, Mingjin Shi, Xiao-Gang Hu*, Yifa Chen*, Shun-Li Li, Ya-Qian Lan

School of Chemistry, Guangzhou Key Laboratory of Analytical Chemistry for Biomedicine, South China Normal University, Guangzhou 510006, China.

ARTICLE INFO

Article history:

Received
Received in revised form
Accepted
Available online

Keywords:

Porous crystalline materials
Multi-metal
Metal-organic frameworks
Covalent organic frameworks
Electrocatalysis

ABSTRACT

Multi-metal porous crystalline materials (MPCM), integrating the functions of both multi-metal centres and porous crystalline materials (e.g., metal-organic frameworks (MOFs) and covalent organic frameworks (COFs)), are an extended class of porous materials that have attracted much attention for a broad range of applications. Owing to the advantages of these materials, they generally display high porosity, multi-metal active sites, well-tuned functions, and pre-designable structures, *etc.*, serving as desired platforms for the study of structure-property relationships. In view of the clean and sustainable target, a series of MPCM have been explored as electrocatalysts for electrocatalytic reactions like hydrogen evolution reaction, oxygen evolution reaction and electrocatalytic CO₂ reduction reaction. Concerning the progress achieved for MPCM in electrocatalytic field during past years, this review will provide a brief introduction on the recent breakthrough of MPCM based electrocatalysts including their synthesis methods, structure design, component/morphology tuning, electrocatalytic property and structure-property relationship, *etc.* Besides, it will also conclude the current challenges and present perspectives for the MPCM based electrocatalysts, which might promote the development of porous crystalline materials in electrocatalysis and hope to provide new insights for scientists in related fields.

1. Introduction

Porous crystalline materials, including metal-organic frameworks (MOFs) and covalent organic frameworks (COFs), are a class of intriguing materials constructed by strong coordination or covalent bonds [1–4]. Owing to the high porosity, crystalline structure, designable function, and homogeneously distributed active sites, they have been regarded as ideal platforms for a series of applications like proton conduction, electro-/photo-catalysis, gas storage/separation and sensing, *etc.* [5–10]. As a kind of porous crystalline materials, MOFs are based on the coordination interaction between metal ion and organic ligand, which possess high porosity, defined structures, and abundant metal sites, *etc.* [11–14]. Meanwhile, COFs, another kind of porous crystalline materials composed of non-metal elements (e.g., C, N, O and B) and connected *via* stable covalent bonds, present unique features like low bulk density, high porosity, adjustable structure/composition, high crystallinity and stability, *etc.* [4,15–18]. Although numerous works have reported their potential applications in catalysis, the current research works are mostly focused on the none or single metal framework structures, which generally lack in diversity or multi-functions to meet the high-performance requirements.

Imparting multi-metal active sites in materials is a promising way to diversify the functionalities and improve the performance of materials. The advantages of multi-metal materials have long been documented in alloy materials [19,20], metal oxides [21–24] and metal hydroxides [25–28]. On one hand, the introduction of foreign metals with different electron affinity can efficiently tune the electron density on the native metal active sites, thus improving the catalysis activity and selectivity [29–32]. On the other hand, effectively correlated multi-metal active sites can bring about synergistic effects or even tandem reactions to realize the synthesis of complex high-valued molecules [33–36]. Especially for the MOFs or COFs, the multi-metal active sites might impart these porous materials with interesting property. Thus obtained multi-metal porous crystalline materials (MPCM) with the imparted two or more metal sites in their structures would offer more opportunity in designing multi-functionality or well-tuned metal sites for varied catalytic applications (Fig. 1) [32,37–41]. Specifically, MPCM may deliver superior property to none or single metal porous materials due to the multi-functionality and complexity derived from the integration of different metal sites in the structures [42–46]. As a result

* Corresponding authors.

E-mail addresses: yirongwang@m.scnu.edu.cn (Y.-R. Wang); huxg@scnu.edu.cn (X.-G. Hu); chyf927821@163.com (Y. Chen).

of the possibly existed synergistic effect that comes from the interaction among two or more metal sites, they might exhibit much more potential with better performance when compared with none or single metal porous crystalline materials [47–51]. It is worth noting that, since MPCM based derivatives are generally obtained by calcination at elevated temperatures, which will result in the collapse of porous crystalline structure, they are sorted as multi-metal materials but out of the scope of this review. This review will focus on the development of MPCM with porous and crystalline structures to discuss their potential in electrocatalytic applications.

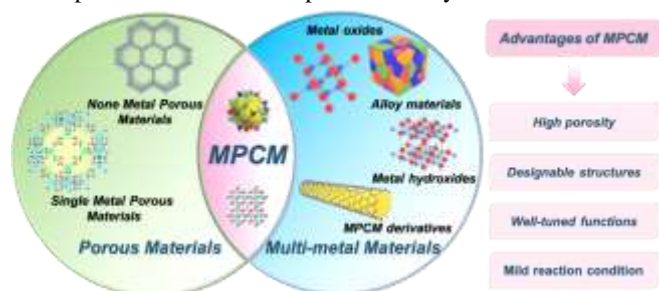


Fig. 1. Classification of porous materials and the advantages of MPCM.

The design of MPCM might replace the traditional none or single metal porous crystalline materials, which can endow the electrocatalysts with higher activity and more available functions to meet the requirements of efficient electrocatalysis [52]. Owing to the high surface area and ordered pore structure, as well as their abundant and varied metal sites, MPCM have aroused much interest in electrocatalytic field owing to the following advantages: (1) The introduction of multi-metal might affect the disorder of crystalline lattice to result in more attractive property [28,43,53,54]; (2) The imparted accessible metal sites (*e.g.*, unsaturated metal sites) in the porous structure would optimize the electron cloud density to improve the electrocatalytic activity; (3) The existed two or more different metal sites in an electrocatalyst might lead to high-entropy alike state in MPCM that can endow diversified microenvironments to boost the performance; (4) The well-defined and designable structures would provide ideal platforms related mechanism investigation [55–58]. In view of these, the exploration of MPCM with new functions that can meet the different requirements of varied electrocatalysis systems is highly demanded and thus this paper will discuss the potentials application of MPCM in electrocatalysis.

The request for sustainable and eco-friendly energy sources causes for the development of advanced energy storage or conversion technology all around the world [59–62]. In particular, electrocatalysis technology powered by renewable electricity provides possibilities for energy conversion and realize the organic synthesis under mild conditions [63–67]. However, electrocatalysis reactions including oxidation (*e.g.*, oxygen evolution reaction (OER), methanol oxidation reaction (MOR)) or reduction ones (*e.g.*, hydrogen evolution reaction (HER), and CO₂ reduction reaction (CO₂RR)) still have some challenges like the energy barriers of catalytic reactions, the competition of side reactions, multi-step mechanistic processes and sluggish reaction kinetics, which needs the specific and complex design of electrocatalysts [68–73]. To meet these requirements, a desirable electrocatalyst needs to display some basic features like high catalytic activity, accessible active sites, efficient charge/mass transfer capability and durability, which causes for the precise design of functional units in electrocatalyst [74–78]. Even more, the varied reaction requirements of the electrocatalytic oxidation or reduction reactions cause for different electron gaining or donating ability of advanced electrocatalysts like MPCM. MPCM, integrating tunable redox multi-metal centers with above-mentioned advantages, hold much promise in these applications (Fig. 2).

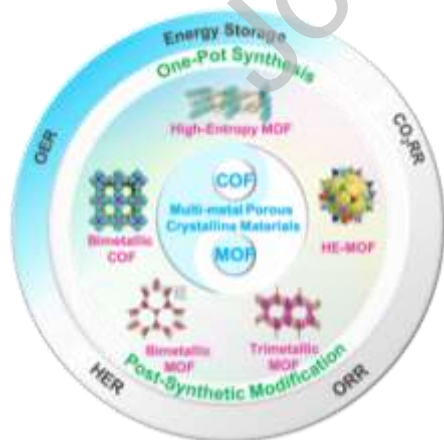


Fig. 2. The schematic representation of the type, synthesis and application of MPCM.

To date, although some noble metals (*e.g.*, Pd, Ir or Ru) have been currently studied as powerful electrocatalysts because of their exceptional performances, the exorbitant price and scarcity still restrict them in large-scale production and practical applications [79–88]. In recent years, significant progress has been made in developing the MPCM based electrocatalysts especially for the last five years (Fig. 3). From 2018, a growing number of MPCM are emerging as important category of advanced porous crystalline materials

for electrocatalysis applications [89,90]. After that, special attention has been paid to the number tuning of metallic elements from two to maximum five as well as the intrinsically electrocatalytic property [69,89–98]. With the increase number of metallic elements in MPCM, the structure of MPCM is more complex with giant diversity of possibly introduced metal types, which has attracted much attention for scientists around the world [99–101]. Up to date, the previously reported reviews mainly focus on none or single metal MOFs or COFs based electrocatalysts and few reviews focused on the MPCM based electrocatalysts [7,10,102,103]. Thus, a timely and systematic review of the preparation strategy, structure, morphology, or electrocatalytic property study for MPCM based electrocatalysts is worthy of attention, which can provide insightful guidance or powerful enlightenment for their applications in electrocatalysis. In this paper, the development, challenge, and perspective of MPCM as electrocatalysts for energy storage and conversion are reviewed (Fig. 3). Recent advances in synthetic strategies, electrocatalytic performance and structure-property relationships of MPCM have been discussed. We hope this review might stimulate widespread interest to further promote the exploration of MPCM in related electrocatalysis fields.

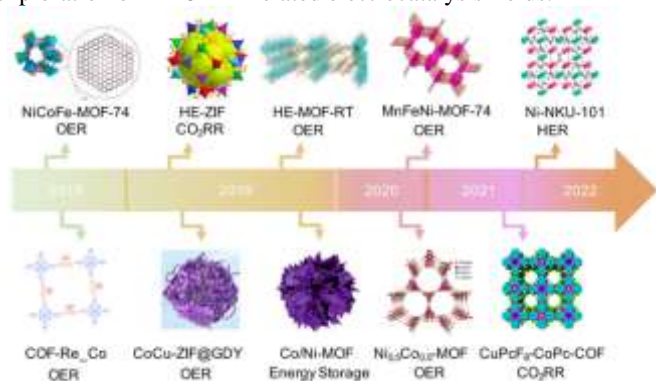


Fig. 3. Evolution timeline and related electrocatalysis applications of MPCM. Reproduced with permission [89–98]. Copyright 2020, Elsevier Inc. Copyright 2019, 2020, 2019, 2022, Wiley-VCH. Copyright 2018, 2018, 2021, ACS. Copyright 2019, RSC. Copyright 2020, Nature.

2. Synthetic strategies for the preparation of MPCM

Up to date, there are two main strategies to synthesize MPCM: One-pot synthesis and post-synthetic modification. At present, most of the synthetic attempts of MPCM focus on one-pot method because of its facile and readily available process [104–106]. In contrast, although the post-synthetic modification method possesses the relatively complex process, it also has advantages like purposefully implanted metal types and higher controllability on the tuning of active metal sites [107–109]. This section will focus on the analysis of these two synthetic methods and in-depth evaluation of their advantages/disadvantages, so as to discuss the practicality of distinct methods and their potential for further applications.

2.1. One-pot synthesis

The reaction of one-pot synthesis can start from relatively simple and easily available raw materials, which can directly transform into products without the separation of intermediates or multi-step treatments, thus improving the overall reaction efficiency [110–114]. The one-pot synthesis method (*e.g.*, hydrothermal, solvothermal, microwave and ball-milling method) using appropriate ratios of varied metal-precursors is promising for the one-pot synthesis of MPCM. It presents the following advantages: (1) Simple synthesis process, the one-pot method enables the facile preparation of MPCM through the direct conversion of precursors; (2) Wide adaptability, MPCM with a variety of crystal structures, nanostructures and compositions can be designed and obtained through this method; (3) Atom economic chemistry, one-pot synthesis is more atom economic when compared with multi-step synthesis process [115–117].

Based on the one-pot synthesis method, Zheng *et al.* have prepared a kind of tetra-metallic FeCoMnNi-MOF-74/NF with a multilevel and hollow nanostructure (Figs. 4a and b) [72]. Briefly, organic linkers and metal salts were added into a mixed solution of N, N-dimethylformamide (DMF), H₂O, and EtOH followed by a solvothermal process at 100 °C for 24 h to give FeCoMnNi-MOF-74/NF. Specifically, the feeding amount and ratio of metal ions (*e.g.*, Fe²⁺, Co²⁺, Mn²⁺) were optimized and FeCoMnNi-MOF-74/NF-1 (Fe²⁺:Co²⁺:Mn²⁺ = 2:3:3), FeCoMnNi-MOF-74/NF-2 (Fe²⁺:Co²⁺:Mn²⁺ = 3:2:3) and FeCoMnNi-MOF-74/NF-3 (Fe²⁺:Co²⁺:Mn²⁺ = 3:3:2) were prepared (Fig. 5).

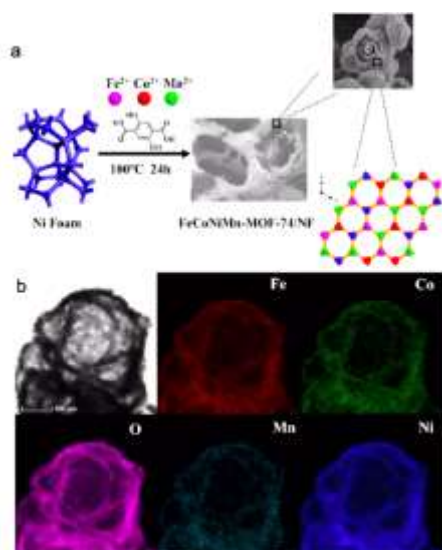


Fig. 4. Structure and characterization of materials. (a) *In situ* growth diagram of FeCoMnNi-MOF-74/NF. (b) TEM image and element map of FeCoMnNi-MOF-74/NF. Reproduced with permission [72]. Copyright 2021, ACS.

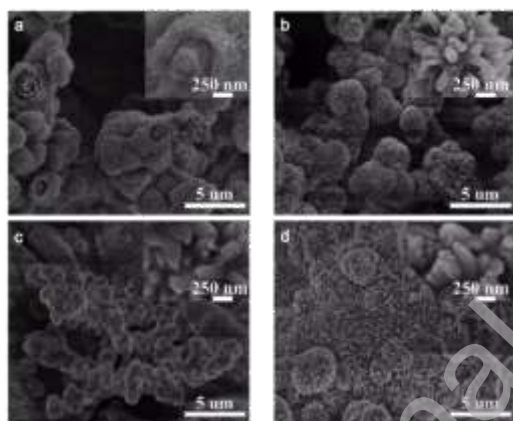


Fig. 5. SEM images of samples. (a) FeCoMnNi-MOF-74/NF. (b) FeCoMnNi-MOF-74/NF-1. (c) FeCoMnNi-MOF-74/NF-2. (d) FeCoMnNi-MOF-74/NF-3. Reproduced with permission [72]. Copyright 2021, ACS.

2.2. Post-synthetic modification

Post-synthetic modification, including methods like the metal exchange or metal insertion, has been regarded as a promising alternative to produce MPCM that cannot be obtained through normal one-pot synthetic methods due to the limitation of different metal reactivity. Besides, the post-synthetic modification can efficiently tune the properties of MPCM for specific applications by controlling the dose of hetero-metal atoms that incorporated into the porous frameworks.

Metal exchange is a readily available post-synthetic modification method for the synthesis of MPCM. For example, Li *et al.* obtained Pd-MOF by metal exchange of the Ni^{2+} site with Pd^{2+} site through a metal exchange post-synthetic modification method (*i.e.*, BUT-33) [118]. The modified material retained the excellent mesoporous property of the original MOF material and exhibited excellent chemical stability. The precise distribution of Pd^{2+} metal sites on atoms had various advantages such as wide application range, high chemical stability, large porosity, and functional controllability. BUT-33(Ni) was immersed in CDCl_3 solutions with Pd(II) at 60 °C to obtain BUT-33(Pd) without single atom Pd and guarantee the crystallinity of the original material (Fig. 6). Thus, skeleton structure and high exchange rate are guaranteed. Energy dispersive X-ray spectroscopy (EDS) element mapping based on TEM reveal the distribution of palladium and nickel in BUT-33(Pd) (Fig. 7a). The Pd element (Pd) in BUT-33(Pd) is evenly distributed throughout the nanocrystals. In addition, the material was characterized by X-ray photoelectron spectroscopy (XPS) to better study the elements of BUT-33(Pd). The results of these characterization above all confirm the successful conversion of Ni^{2+} to Pd^{2+} in the BUT-33 network, rather than the incorporation of Pd nanoparticles or other substances (Figs. 7b-d).

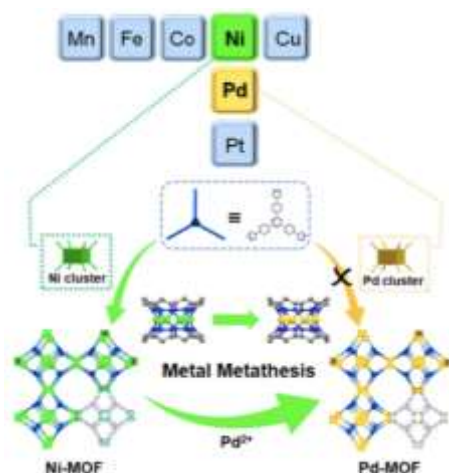


Fig. 6. Metal exchange method for the synthesis of Pd-MOF based on Ni-MOF. Reproduced with permission [118]. Copyright 2021, ACS.

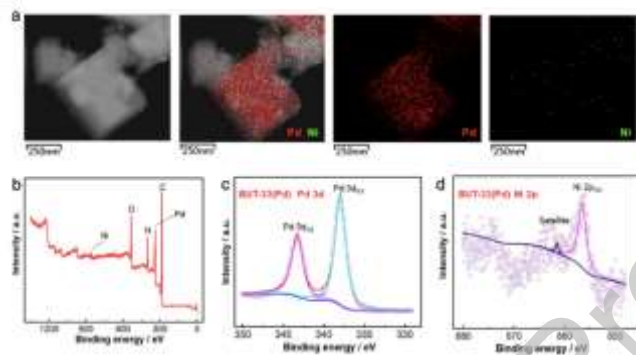


Fig. 7. Characterization of BUT-33(Pd). (a) TEM and elemental mapping images. (b) The XPS spectra. (c) Pd 3d spectra. (d) Ni 2p spectra. Reproduced with permission [118]. Copyright 2021, ACS.

Besides, Du group reported a kind of Ru-doped NiCo-MOF hollow porous nanospheres (Ru@NiCo-MOF HPNs) by using the metal insertion post-synthetic modification method [119]. Ru@NiCo-MOF HPNs with different contents of RuCl_3 can be obtained through this method (Fig. 8). During the experimental process, different amounts of RuCl_3 were added into the suspension of NiCo-MOF HPNs in ethanol under magnetic stirring to accomplish the metal insertion post-synthetic modification process. The resulting Ru@NiCo-MOF HPNs with different Ru doping amounts were obtained by centrifugation.

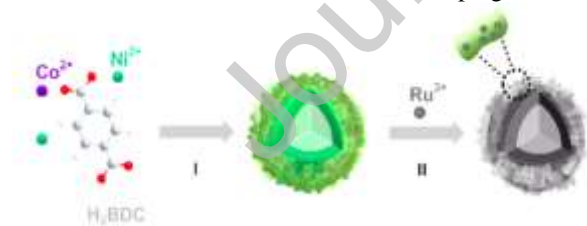


Fig. 8. Synthetic diagram of Ru@NiCo-MOF-4 HPNs through post-synthetic method. Reproduced with permission [119]. Copyright 2021, ACS.

In this reported work, Ru was shown to uniformly distribute on the shell of NiCo-MOF HPNs while Ni, Co and O dispersed in the body. The ultra-low dose of Ru with high OER activity on the exposed surface of NiCo-MOF HPNs can further improve catalytic performance of the bimetallic catalyst. In addition, the MOFs precursor helps to maintain the original hollow spherical structure after electrochemical test, ensuring its good catalytic stability (Fig. 9). The work not only shows the successful incorporation of Ru on the surface of NiCo-MOFs through the metal insertion post-synthetic modification method, but also proves the high OER performance and stability of thus-obtained electrocatalyst.

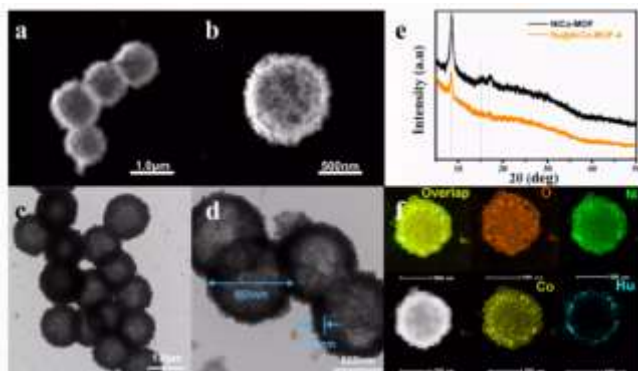


Fig. 9. HAADF-STEM images of (a) NiCo-MOF HPNs and (b) Ru@NiCo-MOF-4 HPNs. TEM images of (c) NiCo-MOF HPNs and (d) Ru@NiCo-MOF-4 HPNs. (e) XRD patterns. (f) Elemental mapping images of Ru@NiCo-MOF HPNs. Reproduced with permission [119]. Copyright 2021, ACS.

In addition to these, the metal insertion post-synthetic modification method is also applicable to produce bimetallic COFs material. For example, Wang *et al.* have synthesized a kind of covalent organic skeleton-supported bimetallic nano-catalysts (Cu/Ag-COF) (Fig. 10a) [120]. Initially, COFs was first synthesized by Schiff base condensation reaction at room temperature. Porous COFs can provide rich sites for the loading of metal nanoparticles. Then, the Cu/Ag-COF bimetallic nano-catalysts were further prepared by the post-synthetic reduction reaction of metal nanoparticles on COFs. The Cu/Ag-COF synthesized by post-modification can be further characterized. Based on the SEM and TEM tests, the COFs prepared by this method is spherical and the size is about 1 μm. The fixation of metal nanoparticles did not change the morphology of COFs. Besides, the EDS mapping of Cu/Ag-COF showed that Ag and Cu elements were uniformly dispersed on the COF nanosphere, further confirming that metal nanoparticles are successfully loaded onto the COFs (Figs. 10b-g).

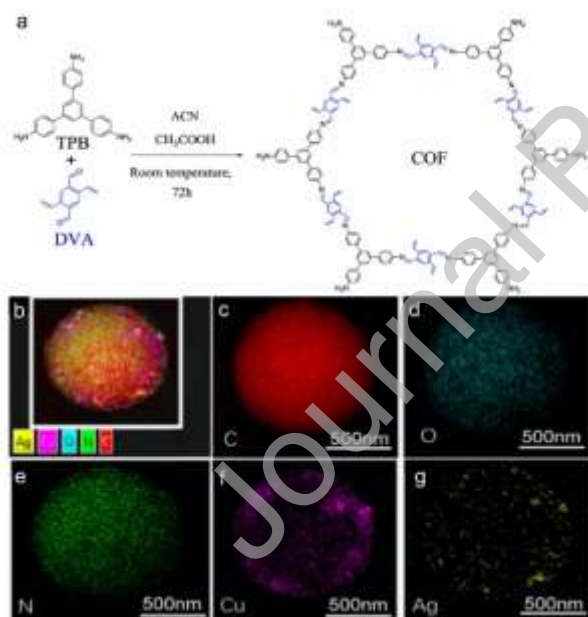


Fig. 10. Preparation and characterization of Cu/Ag-COF. (a) Synthesis process of Cu/Ag-COF. (b-g) Element mapping of Cu/Ag-COF. Reproduced with permission [120]. Copyright 2022, Elsevier Inc.

3. Applications of MPCM in electrocatalytic oxidation reaction

In general, MPCM with multi-metal sites presents much opportunities to integrate the diversity and synergistic effects due to the existence of abundant metal sites. This is reflected by their more superior performances or higher stability to their none or single metal counterparts. Electrocatalytic oxidation reactions are a class of important catalysis technology that can convert low-value substrates into more valuable products through the electron transfer process [121–123]. In this section, the electrocatalytic oxidation reactions (*e.g.*, OER and MOR), a class of important catalysis reactions that can convert low-value substrates into more valuable products through the electron transfer processes are reviewed sequentially [124–128]. The superiority of MPCM as advanced electrocatalysts for energy storage and conversion are described and discussed in detail.

3.1. The applications of MPCM in OER

OER is a kind of important electrocatalytic reaction that plays vital roles in a series of applications like water splitting, metal-air batteries, and fuel cells [129–132]. However, the sluggish kinetics of the four electrons and four protons process of OER suppresses the high-efficiency energy conversion. Therefore, it is important to design efficient electrocatalysts to advance reaction kinetics and improve OER catalytic activity [129–132]. During past years, MPCM have exhibited high electrocatalytic activities in OER and a large number of interesting works have been reported [133–136]. The following section will discuss the recent development of MPCM in OER based on the classification from bimetallic MOFs to high-entropy MOFs.

3.1.1. Bimetallic MOFs

Bimetallic MOFs, as a kind of traditional MPCM, have been commonly investigated in the fields of energy storage and conversion. Compared with single metal porous crystalline materials, the inherited advantages of porosity together with inherent multi-metal coordination of bimetallic MOFs can greatly improve their performances in electrocatalysis [44]. This chapter will review the latest research progress of bimetallic MOFs used in electrocatalytic OER reactions.

Based on the proper choice of metal ions, diverse frameworks have been applied to construct MPCM. Among them, Prussian blue is an ideal platform to construct bimetallic MOFs. The Prussian blue analogue (PBA) produced by replacing Fe ions with a second metal can generate promising electrocatalytic performance [137]. For example, Zhang *et al.* reported a bimetallic PBA, Ni-Fe-PBA, as electrocatalyst for OER under alkaline conditions [138]. The results showed that Ni ions could be completely converted into Ni hydroxide by the electrochemical treating process, in which $\text{Ni}(\text{OH})_2$ would serve as the active substance for OER. Operando X-ray spectroscopy studies further showed that the *in-situ* formed $\text{Ni}(\text{OH})_2$ exhibited a unique property to allow the deprotonation to be occurred at an applied potential to produce NiOOH_{2-x} containing Ni^{4+} ions. Specifically, the deprotonation process was potential dependent and reversible and, during which the Ni^{4+} amount enhanced with the increase of potential. The *in-situ* activated sample has a low overpotential of only 258 mV at 10 mA/cm^2 . At the overpotential of 304 mV, the current density could reach up to 61 mA/cm^2 , which was about 6 times higher than that of IrO_2 (10 mA/cm^2). DFT calculations showed that Ni^{4+} served as a trigger for the oxygen-oxide ion to act as the electrophilic center to subsequently activate the anionic redox reaction of OER.

Another bimetallic Prussian blue was adopted by Gong *et al.* [133]. They prepared a kind of S-treated two-dimensional (2D) CoFe bimetallic PBA (S-CoFe-PBA/CFP) on carbon fiber paper (CFP) as an electrocatalyst for high-efficiency OER at alkaline conditions (Fig. 11a). The reasons for the high performance are as follows: (1) The favorable factors, including the 2D nanosheet structure and conductive substrate CFP, impart higher starting point for the whole system; (2) The electron interaction between the amorphous CoS_x and Fe-PBA nanosheets would be much beneficial for the absorption of intermediates in OER and charge transfer; (3) $-\text{SO}_x$ continues to capture H^+ from intermediates of $^*\text{OH}$ and $^*\text{OOH}$ on the catalyst surface, resulting in rapid OER progress and reduced activation energy. The OER catalytic activity of the synthesized S-CoFe-PBA/CFP was significantly improved. Driving current densities of 10, 50, and 100 mA/cm^2 require only 235, 259, and 272 mV of overpotential (Figs. 11b and c), and the ultra-low Tafel slope is 35.2 mV/dec. More notably, when 1.5 V vs. RHE potential is applied, a current density of 90 mA/cm^2 can be achieved.

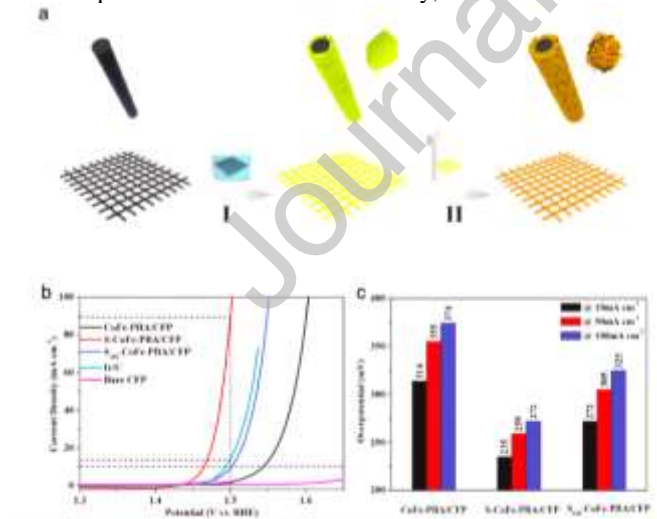


Fig. 11. Synthesis and electrocatalytic performance of materials. (a) Schematic diagram of S-CoFe-PBA/CFP synthesis process. (b) Linear polarization curves. (c) Overpotential at different current density. Reproduced with permission [133]. Copyright 2020, RSC.

Except for PBA, zeolitic imidazolate frameworks (ZIFs) have also been utilized to synthesize the bimetallic MOFs (*i.e.*, CoCu-ZIF) [96]. For instance, the CoCu-ZIF@GDY nanomaterials was synthesized by post-synthetic modification using CoCu-ZIF NSs and graphite-alkyne (GDY) (Fig. 12a). Compared with GDY nanowire, its content of adsorbent O is higher than that of GDY nanowire, indicating that it has higher OER electrocatalytic activity. In addition, one-dimensional GDY nanowires have highly

conjugated structures and contain a large number of carbon points. Due to the interaction between the carbon skeleton of GDY and the active catalyst metal site of CoCu-ZIF NSs, the OER performance of CoCu-ZIF@GDY is significantly better than that of the individual components of CoCu-ZIF and GDY. CoCu-ZIF@GDY nanomaterials demonstrated superior OER properties with a 250 mV overpotential at a current density of 10 mA/cm² (Figs. 12b and c). When applied as an electrolytic cell catalyst for water splitting in two-electrode system, it also showed a low cell voltage of 1.52 V at 10 mA/cm² and high stability.

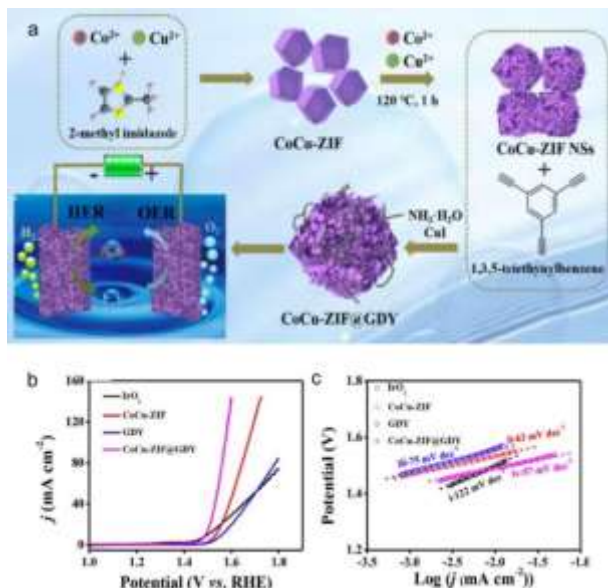


Fig. 12. Synthesis and electrocatalytic performance of materials. (a) Formation of CoCu-ZIF@GDY. (b) LSV curves. (c) Tafel plots. Reproduced with permission [96]. Copyright 2020, Elsevier Inc.

Moreover, Tang *et al.* have fabricated a kind of bimetallic MOFs (Ni_{0.9}Fe_{0.1}-MOF) during the OER process [97]. A potential-induced two-step structural transformation was observed at the metal nodes during the OER process on NiCo-MOF-74, including an activation process to produce oxyhydroxide from hydroxide under potential and further conversion process into NiCo-MOF-74 after the potential is removed. Furthermore, the catalytic activity can be adjusted by changing the Ni/Co ratio. Based on the above principle, Ni_{0.9}Fe_{0.1}-MOF was fabricated and achieved high OER activity. It exhibits a low overpotential of 198 mV at 10 mA/cm² and 231 mV at 20 mA/cm², respectively (Fig. 13). Besides, Fu *et al.* synthesized MOF-74 (Cu/Co) as catalyst for the applications of styrene oxidation [139]. The catalytic performance of MOF-74 (Cu/Co) can be adjusted by changing the Cu/Co ratio in MOF-74. Interestingly, the MOF-74 (Cu/Co) catalyst showed superior activity in the styrene oxidation reaction to the physical mixture of MOF-74 (Cu) and MOF-74 (Co) with almost identical Cu and Co contents. Therefore, the higher activity of MOF-74 (Cu/Co) catalyst can be attributed to the synergistic interaction of Cu²⁺ and Co²⁺ active sites. Surprisingly, the incorporation of Cu²⁺ into MOF-74 (Co) completely inhibited the polymerization of styrene, while the introduction of Co²⁺ into MOF-74 (Cu) promoted the reaction from styrene to benzaldehyde, epoxy-styrene and phenacetaldehyde. Besides, the increase of Co²⁺ amount in MOF-74 (Cu/Co) could enhance the conversion of substrate, improve the selectivity of epoxide styrene and phenacetaldehyde, and reduce the selectivity of benzaldehyde.

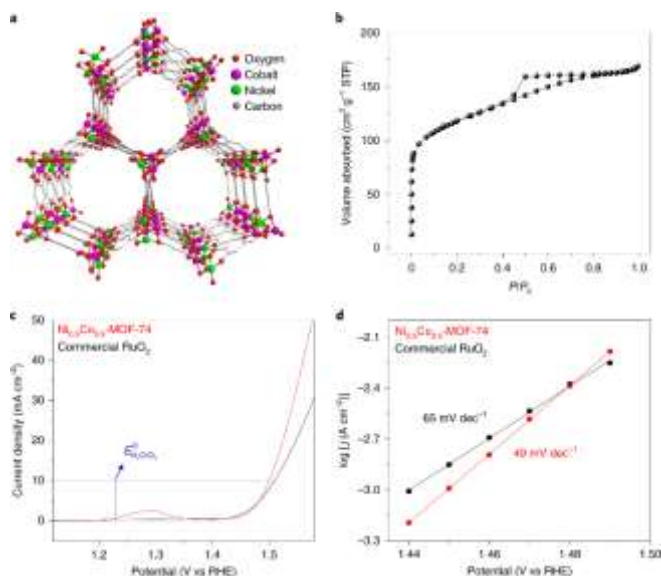


Fig. 13. (a) Structure of $\text{Ni}_{0.5}\text{Co}_{0.5}\text{-MOF-74}$. (b) N_2 isotherm of $\text{Ni}_{0.5}\text{Co}_{0.5}\text{-MOF-74}$. (c) $\text{Ni}_{0.5}\text{Co}_{0.5}\text{-MOF-74}$ and commercial RuO_2 . (d) Tafel diagram. Reproduced with permission [97]. Copyright 2020, Nature.

In contrast to the conventional strategy to synthesize MOFs with high crystallinity, Li *et al.* constructed low crystalline bimetallic MOFs (*i.e.*, $\text{Fe}_1\text{Ni}_2\text{-BDC}$) when inducing foreign metal ions [140]. Interestingly, the introduction of Ni ions led to the coordination mismatch with the organic ligand and defective pore structure for $\text{Fe}_1\text{Ni}_2\text{-BDC}$. The obtained structure possessed abundant local crystallinity defects, which largely enhanced the mass transport and accessible sites. In addition, the distance of Ni-O in $\text{Fe}_1\text{Ni}_2\text{-BDC}$ is larger than that of Fe-O, and the Fe-O bond itself also has a small increase when Ni^{2+} ions are introduced into the Fe-BDC framework. When used as a kind of OER electrocatalyst, the low-crystal bimetallic MOFs presented a low 260 mV overpotential at 10 mA/cm^2 and a 99.5% Faraday efficiency.

Although bimetallic catalyst has been widely applied in OER, the reason for its improved performance remains elusive. To study it, Lan *et al.* have designed and synthesized a series of stable bimetal-organic framework to explore the OER mechanism (Fig. 14a) [141]. The optimized NNU-23 displayed the highest OER performance with a 365 mV overpotential at 10 mA/cm^2 , which is superior to most of the MOF-based electrocatalysts in 0.1 mol/L KOH (Figs. 14b-d). Specifically, all bimetallic MOFs showed improved OER activity compared to monometallic MOFs. DFT calculations show that the introduction of extra metal can bring the d-band center closer to Fermi level and form stronger binding interactions between the adsorbate and catalyst, thus improving the OER performance.

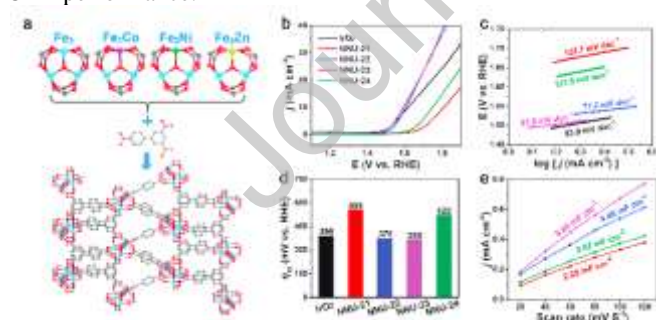


Fig. 14. Crystal structure and electrocatalytic OER performance of NNU-21-24. (a) 3D framework. (b) LSV curves. (c) Tafel plots. (d) Overpotential at 10 mA/cm^2 . (e) Plots for C_{dl} . Reproduced with permission [141]. Copyright 2018, Wiley-VCH.

Except for the choice of metal ions and framework structure, adjusting morphology is also an alternative method to enhance the electrocatalytic property of MPCM. Dong *et al.* developed an *in situ* self-dissociation-assembly method for the one-pot preparation of 3D ultra-thin CoNi-MOF nanosheet arrays (CoNi-MOFNA) that can be applied as highly active OER catalyst [142]. Electrochemistry and time-varying XAS techniques clearly indicate that the activity and structural evolution is caused by the synergistic interaction of bimetallic electronic coupling and the active site of the coordinated unsaturated atom. This strategy has also been shown to be effective for the control of thickness and height that can also be available for the large-scale fabrication of various types of ultra-thin MOFs nanosheet arrays on different substrates. Compared with the bulk CoNi-MOF, CoNi-MOFNA and

CoNi-MOFNS have larger surface area, which significantly improves the OER activity. Besides, the activity of CoNi-MOFNA is much higher than that of CoNi-MOFNS, which may be ascribed to the tight interaction with the conductive substrate and ordered array structure. Moreover, CoNi-MOFNA displayed a 10 mA/cm² current density at a 215 mV overpotential and showed negligible attenuation even after 300 h reaction. Notably, its mass activity could be 14 times larger when compared with commercial RuO₂.

Apart from the electrocatalysis, energy storage is also a promising application for bimetallic MOFs. Jiao *et al.* reported the preparation of [Ni_{3-x}Co_x(OH)₂(tp)₂(H₂O)₄]·2H₂O (X = 0.69) (Co/Ni-MOF) by partial substitution of Ni²⁺ in Ni-MOF with Co²⁺ via a hydrothermal process [143]. It still retained the crystal structure of Ni-MOF, and could deliver electron and ion transport pathways, which is beneficial for the storage of electrolyte ions. Specifically, Co/Ni-MOF//CNT-COOH presented high energy density (49.5 Wh/kg) and power density (1450 W/kg). The superior property would be ascribed to the synergistic interaction of integrated mixed metal sites that can enhance the conductivity and surface area of MOFs, henceforth providing a favorable path for charge transport and improving the electrochemical double-layer capacitance (EDLC) with the increase of surface area.

In addition to the common transition metal elements, lanthanides can also be used as synthetic materials for polymetallic MOFs. Aghazadeh *et al.* cultured a spherical mixed thulium/samarium metal MOFs (*i.e.*, Tm, Sm-IMC-MOF) uses 1-imidazol-carboxylate (IMC) as an organic connector on a Ni-foam (NF) porous carrier [144]. This new strategy can be simply used to prepare one - or multi-component MOFs materials in aqueous media for different applications. The properties of synthetic materials can also be adjusted by changing the electrodeposition environment. Tm, Sm-IMC-MOF/NF electrodes had good electrochemical properties. The assembled material device presented a specific capacity of 239 C/g at 4 A/g and a surface capacity of 2.11 C/cm², with a capacity retention rate of 63% at current density from 1 A/g to 20 A/g. Notably, Tm, Sm-IMC-MOF based electrode can provide a suitable specific capacity of 645 C/g at 1 A/g. After 5000 cycles at 4 and 8 A/g, the cycle retention rates of the assembled ASC devices were 85.4% and 91.5%, respectively. In addition, EIS data show that Tm, Sm-IMC-MOF have lower internal resistance and lower electron/electrolyte transport resistance at NF electrodes. Subsequently, Aghazadeh *et al.* prepared tubular and secondary sea urchin-like bimetallic samarium/thulium nitrate organometallic skeletons (ST-MOF). As electrode material, ST-MOF has high specific capacity, good cycle life and excellent high rates performance. The high performance is attributed to its good battery type behavior [145]. When applied in supercapacitor, high capacitance of 511 C/g and 419 C/g can be obtained for ST-MOF@NF based electrode when the current density is 10 A/g and 50 A/g. With the current density increases from 5 A/g to 100 A/g, a 64.6% amplification capacity is obtained. At 10 A/g and 50 A/g current loads, the initial capacitance stability of ST-MOF@NF electrode after 12000 galvanostatic charge/discharge cycle is 93.25% and 75.18%, respectively.

In related applications in the battery field, the aforementioned NiCo-containing metal MOFs also have superior performance for energy storage. He *et al.* synthesized a series of iso-structured Co-Ni-MOF by a simple method in the presence of Co/Ni mixed metal ions with different molar ratios [146]. The storage capacity of Li⁺ can be improved by doping Co ion in Ni-MOF. The enhanced properties of Co-Ni-MOF materials are mainly due to the synergistic effect of the two kinds of metal sites, the improvement of electron/ion conductivity, the enhancement of structural stability, which ultimately guarantee the high performance. Specifically, the Co-Ni-MOFs electrodes with optimized Co/Ni molar ratio showed a specific capacity of 800 mAh/g, with 98% maintained after 100 cycling at 100 mA/g.

Lu *et al.* synthesized a Ni/Co hybrid MOFs with hierarchical spherical structure by hydrothermal method (*i.e.*, Ni/Co-MOF) [147]. By adjusting the molar ratio of Ni/Co and ligand, the morphology evolution and performance optimization of hybrid MOFs were intensively studied. The Ni/Co hybrid MOFs as electrode exhibits better electrochemical performance than the mono-metal MOFs, and its morphology can be adjusted by tuning the Ni/Co ratio. The structure and the corresponding capacity of the mixed MOFs showed a pattern, in which the MOFs with Ni/Co = 1:2 (referring to the mixing ratio of Ni and Co during the synthesis process) had the best capacity. At 1 A/g, the specific capacity of Ni/Co-1:2 is as high as 339.3 C/g and maintained 70.3% after 2000 cycles. In addition, the prepared two-electrode cells displayed energy densities of 12.8 Wh/kg at 372.5 W/kg and 5.8 Wh/kg at 6760 W/kg, respectively.

3.1.2. Trimetallic MOFs

In addition to the relevant exploration of bimetallic MOFs in the field of electrocatalysis, trimetallic MOFs can further optimize the performance of electrocatalysis in terms of synergistic effects. Remarkable progress was made in the fields of OER by introducing trimetallic units in MOFs and regulating their morphology [148]. Compared with bimetallic MOFs, trimetallic MOFs might further enhance the reaction activity and performance, which may be due to the enhanced adsorption energy of intermediates and more active centers. The literatures reported include MOF-74, PBA, Materials of Institut Lavoisier (MIL) MOFs, *etc.* [149]. Thus, we will focus on trimetallic MOFs to review their relevant applications in electrocatalysis.

For example, Lang *et al.* have synthesized a series of trimetallic MOFs (FeNiCo-MIL-53) through a solvothermal method that can be used as a high efficiency OER electrocatalyst [150]. The optimized FeNi_{2.4}Co_{0.4}-MIL-53 showed overpotentials of 219 mV and 236 mV at 10 mA/cm² and 20 mA/cm², respectively. Besides, FeNi_{2.4}Co_{0.4}-MIL-53 can provide 79.6 mA/cm² for OER at 1.50 V (relative to RHE), twice as much as FeNi_{2.4}-MIL-53 (33.6 mA/cm²), making it one of the best electrocatalysts for OER reported to date. Because the active centers of FeNi_{2.4}Co_{0.4}-MIL-53 was evenly distributed, the existed Fe, Co and Ni could modulate the inherent property to improve the OER performance.

Besides, Zhang *et al.* successfully prepared MOFs (*i.e.*, FCN-BTC MOF) with unique chrysanthemum nanoflower structure on Ni foam (NF) by a simple one-pot solvothermal strategy [71]. Notably, the catalyst only required overpotentials of 218, 250 and 268 mV to obtain current density of 10, 100 and 300 mA/cm² for OER, respectively, in 1 mol/L KOH solution. In addition, the loss of current density was only 3.5% after 24 h reaction at 50 mA/cm². Moreover, stronger synergistic effects can also be observed in trimetallic MOF-74 than its bimetallic counterparts. For example, Hu *et al.* modulated the electronic structure of Mn_{0.52}Fe_{0.71}Ni-MOF-74 by imparting Mn into bimetallic MOF-74 (Fig. 15a) [93]. In the electrocatalysis process, Mn can be used as a precursor of high energy metal intermediate for the products stabilized by the redox regulator, thus facilitating the electrocatalysis. The optimized Mn_{0.52}Fe_{0.71}Ni-MOF-74 thin film electrode exhibited high performance, with current density of 10 mA/cm² at HER overpotential of 99 mV and 100 mA/cm² at OER overpotential of 267 mV. As a bifunctional catalyst, Mn_{0.52}Fe_{0.71}Ni-MOF-74 thin film electrode presented superior water splitting performance, with low overpotentials of 245 and 462 mV at current density of 10 and 100 mA/cm², respectively (Fig. 15b-e).

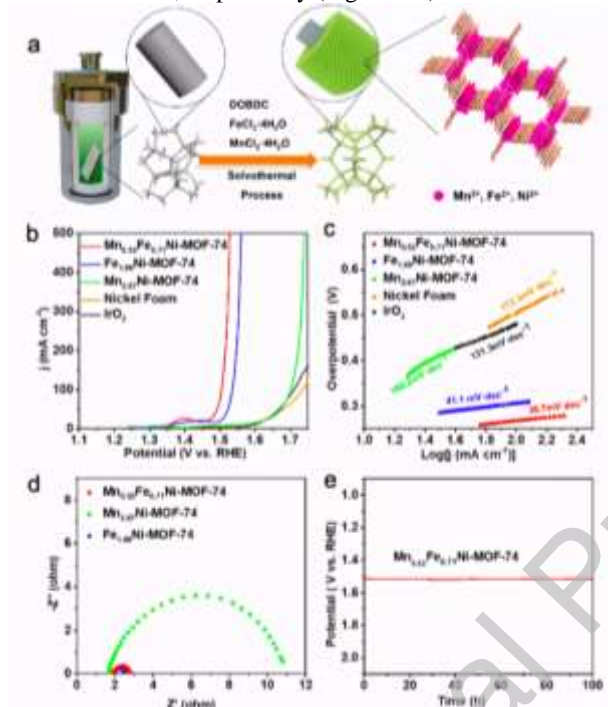


Fig. 15. Synthesis and electrocatalytic performance of Mn_{0.52}Fe_{0.71}Ni-MOF-74 on nickel foam (NF). (a) Preparation process of Mn_{0.52}Fe_{0.71}Ni-MOF-74. (b) OER properties. (c) Tafel diagrams. (d) Nyquist diagram. (e) Long-time stability. Reproduced with permission [93]. Copyright 2020, Wiley-VCH.

Additionally, Li *et al.* explored a partial pyrolysis method in which a solid NiCo/Fe₃O₄ heteropatric was constructed in the NiCoFe-MOF-74 as a precursor to achieve efficient OER (Fig. 16a) [90]. The method preserved the skeleton structure of MOFs while preparing highly active nanoparticles, which is conducive to the effective diffusion of substrates. The electrocatalytic properties of the samples were tested in 1 mol/L KOH. NiCoFe-MOF-74 with the element ratio of Ni:Co:Fe = 1:2:1 exhibited an overpotential of 270 mV at 10 mA/cm², which exceeds the overpotential of monometallic (*i.e.*, Ni-MOF-74, Co-MOF-74 and Fe-MOF-74) and bimetallic counterparts (*i.e.*, NiCo-MOF-74, NiCo-MOF-74 and CoFe-MOF-74) (Fig. 16b). Additionally, the Tafel diagram illustrates the reaction mechanism (Fig. 16c).

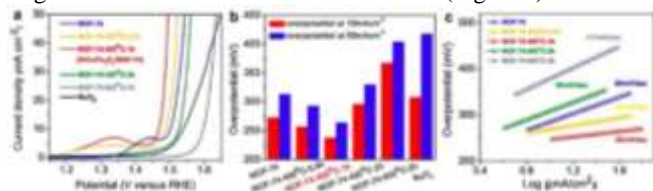


Fig. 16. Electrocatalytic performances of NiCoFe-MOF-74. (a) LSV curves. (b) The overpotentials at the current density of 10 and 50 mA/cm². (c) Tafel slope. Reproduced with permission [90]. Copyright 2018 ACS.

Kundu *et al.* have synthesized a series of trimetallic ZIFs *via* a wet chemical strategy [151]. After the introduction of metals into the porous framework, this powder sample was fabricated into fibers (CoNiFe-ZIF-MFs) through electrospinning. The overpotential value of CoNiFe-ZIF-MFs was 273 mV at 10 mA/cm², indicating that the catalyst had a high electrochemical OER activity. This

result is comparable to that of commercial RuO_2 and NiO catalysts. The overpotential values of RuO_2 and NiO catalysts at 10 mA/cm^2 were 265 mV and 309 mV, respectively. It is clear from this study that the presence of the Ni, Co and Fe possesses synergistic effect on the improvement of OER activity and extended stability.

Prussian blue has also been applied as trimetallic MOFs in electrocatalytic applications. For instance, Wang *et al.* prepared 2D-3D nanostructures with metal hydroxide and PBA *in-situ* growth onto NiFe foam (Pt-NiFe PBA) using a simple and scalable corrosion coordinate method (Fig. 17a) [69]. With a contact angle of 0° , Pt-NiFe PBA exhibits super hydrophilicity, which facilitates the close contact with electrolyte or electrode and maximizes the reaction sites to accelerates the kinetics. The specially designed morphology is conducive to providing sufficient reaction sites, optimizing reaction pathways and accelerating mass transfer during electrocatalysis. The synthesized Pt-NiFe PBA required overpotentials of 29 and 210 mV for HER and OER to achieve 10 mA/cm^2 in 1 mol/L KOH deionized water, respectively (Figs. 17b and c). In seawater containing 1 mol/L KOH, Pt-NiFe PBA requires an overpotential of 21 mV to drive 10 mA/cm^2 and has superior durability. In addition, using Pt-NiFe PBA as the bifunctional electrocatalyst, the voltage required to drive 10 mA/cm^2 in 1 mol/L deionized water KOH and 1 mol/L seawater KOH is 1.46 V and 1.48 V, respectively.

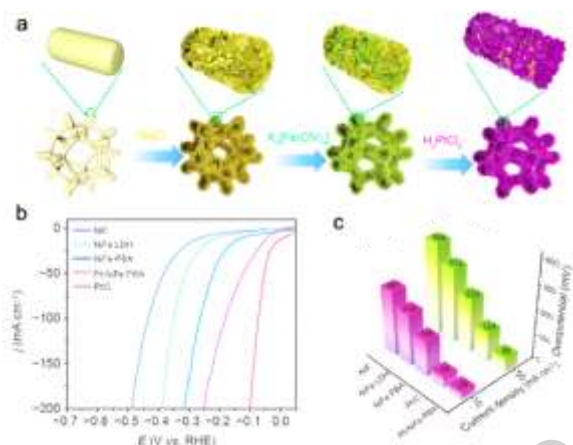


Fig. 17. Synthesis and electrocatalytic performance of Pt-NiFe PBA. (a) preparation process of Pt-NiFe PBA. (b) HER performances in 1 mol/L KOH. (c) Overpotentials at 10 and 50 mA/cm^2 . Reproduced with permission [69]. Copyright 2021, Science Press.

Apart from the electrocatalysis, trimetallic MOFs can also be applied in energy storage. Shi *et al.* synthesized a regular micron rod-like Ni, Fe, Mn benzene-1,2,4,5-tetracarboxylic acid trimetallic organic skeleton (NiFeMn-PMA) and explored the performance of lithium ions batteries (LIBs) [70]. Trimetallic MOFs (NiFeMn-PMA) showed higher rate properties than single-metal MOFs (Ni-PMA) and bimetallic MOFs (NiFe-PMA), which was ascribed to the synergistic interaction of polymetallic mixed sites. Notably, NiFeMn-PMA based cathode shows high capacity of 802.1 mAh/g and good cycle stability (624 mAh/g for 100 mA/g over 100 cycles) in LIBs. Meanwhile, after 100 cycles, holes are formed on the surface of the NiFeMn-PMA electrode, which can largely accelerate the interaction between electrolyte and electrode, deliver abundant sites for Li storage and facilitate the Li^+ migration.

3.1.3. HE-MOF

Based on the above research, there are more metal-doped MOFs materials such as five-membered metal MOFs, which is often referred to as high-entropy (HE) like MOFs. HE materials commonly exhibited unique characteristics, tunable compositions, and high physicochemical properties. Zhang *et al.* proposed an one-step solvothermal method to synthesize a high entropy like MOFs (HE-MOFs) [73]. The EDS spectra of metal-rich HE-MOFs showed that C, O, S, Fe, Co, Ni, Mn, Cu and other elements were evenly distributed. HE-MOFs with high specific surface has more electrochemically active sites, which accelerate the mass transfer and reaction kinetics of OER process. The results show that the HEMOF lattice distortion caused by the introduction of polymetallic ions leads to an increase in OER activity compared to the original MOFs of a single metallic site. Notably, the overpotential of the optimized Co-HE-MOF is 310 mV at the current density of 10 mA/cm^2 , which is better than that of RuO_2 catalyst under the same conditions. More importantly, the introduction of multi-metals with different radii/valences alters the coordination environment around the catalytic atoms, showing the presence of oxygen defects, thereby increasing OER activity by altering the electronic structure and thus affecting the desorption-absorption strength of oxygen intermediates.

Mu *et al.* reported a class of HE-MOFs synthesized from a mixture of five metals (Mn^{2+} , Fe^{3+} , Co^{2+} , Ni^{2+} , and Cu^{2+}) and 1, 4-benzodicarboxylic acid (1, 4-BDC) [95]. Five components of high entropy metal-organic skeleton were synthesized by solid phase method at room temperature. The results show that all the metal ions in the obtained HE-MOFs are randomly dispersed and nearly equimolar distribution, which indicates that HEMs are successfully formed by solid phase method. Specifically, the overpotential

(245 mV) for OER of the prepared HE-MOF-RT was superior to those of HE-MOF-ST (293 mV) and commercial RuO_2 (346 mV) at 10 mA/cm^2 (Fig. 18).

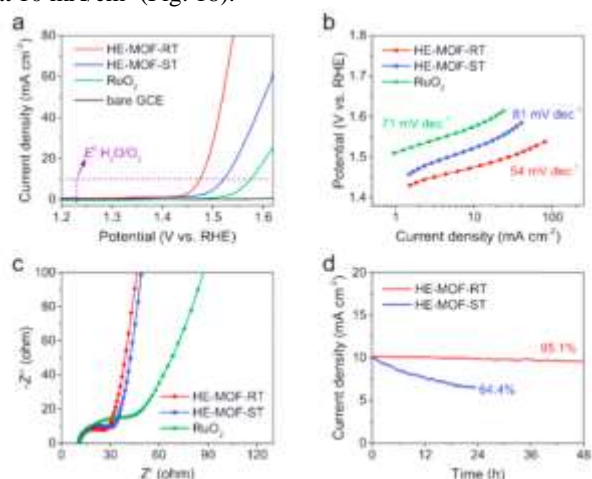


Fig. 18. Electrocatalytic performance of HE-MOF-RT. (a) LSV polarization curves. (b) Tafel plots. (c) EIS curves. (d) Long-time stability at 10 mA/cm^2 . Reproduced with permission [95]. Copyright 2019, RSC.

Chen *et al.* prepared HE-MOFs containing Ni, Co, Fe, Zn and Mo by a mild solvothermal way. HE-MOFs was composed of 2, 6-naphthalene dicarboxylate and inorganic metallic oxygen layers, with each metal ion in octahedral coordination (Fig. 19a) [152]. HE-MOFs presented a 2D array structure that could both improve the conductivity and facilitate the mass transport. In addition, the synergistic effect of different metals contributes to the entropy-increasing effect, which drives efficient OER performances. HE-MOFs showed the best electrocatalytic OER activity with can remain stable up to 100 h. Interestingly, HE-MOFs required a minimum overpotential of 254 mV to drive the current density of 50 mA/cm^2 , which was better than Fe-MOF (277 mV), NiFe-MOF (357 mV), NiFeZn-MOF (289 mV), NiFeZnMo-MOF (265 mV), NF (549 mV) and IrO_2 (346 mV) (Figs. 19b and e). Additionally, the Tafel diagrams of main samples and contrast samples are shown in Fig. 19c to detect changes in reaction mechanism. This kind of HE-MOFs also has a relatively small impedance (Fig. 19d).

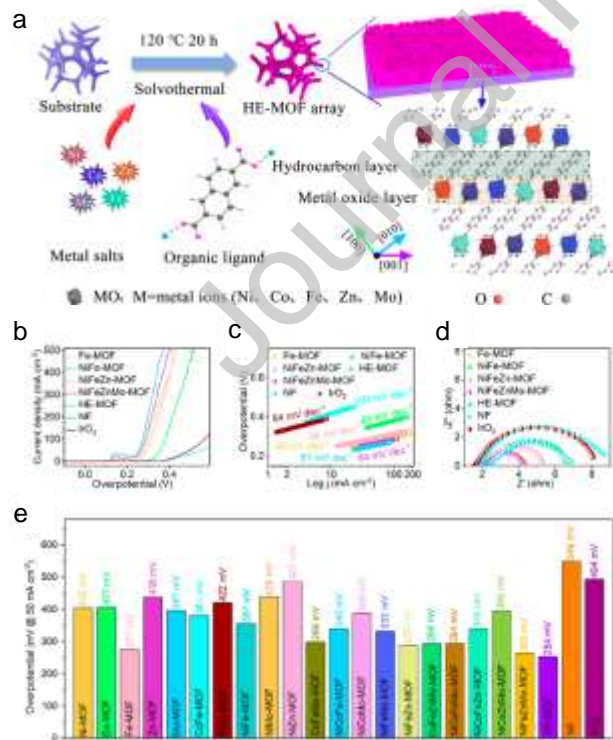


Fig. 19. Synthesis and electrocatalytic performance of 2D HE-MOFs array. (a) Synthetic illustration of the 2D HE-MOFs array. (b) LSV curves. (c) Tafel plots. (d) Nyquist plots. (e) The overpotential at 50 mA/cm^2 . Reproduced with permission [152]. Copyright 2022, ACS.

3.1.4. Bimetallic COFs

The research on MOFs materials has reached a relatively mature stage, but the research on COFs has remained in a relatively preliminary stage since 2005 [4]. Therefore, the multi-metallic COFs materials reported so far are all based on binary metals, and their applications are relatively preliminary. We summarized the applications related to binary metal COFs, mainly including $\text{Fe}_{0.5}\text{Co}_{0.5}\text{Pc-CP}$, COF-Re-Co and so on.

Yao *et al.* reported a series of 2D conjugated materials (CPs) nanosheets with fully conjugated electronic structures (*i.e.*, $\text{Fe}_{0.5}\text{Co}_{0.5}\text{Pc-CP}$) through the exfoliation of ethynyl-linked phthalocyanine (Pc) CPs (MPc-CPs, $\text{M} = \text{Fe}, \text{Co}, \text{Fe}_{0.5}\text{Co}_{0.5}$) [153]. It exhibited a layered structure with abundant inherent structural defects and highly disordered frame properties. Specifically, $\text{Fe}_{0.5}\text{Co}_{0.5}\text{Pc-CP NS@G}$ showed excellent zinc-air battery activity with an open-circuit voltage of 1.34 V and a peak power density of about 180 mW/cm². Its high performance is ascribed to the accessible active centers with synergistic interaction in the two-dimensional nanolayer and the high electron transfer capacity of graphene NSs.

Noble metals like Au or Ag can also act as intrinsic metal sites for better performance. Wang *et al.* synthesized a Cu/Ag bimetallic nanoparticles supported covalent organic skeleton (Cu/Ag-COF), which showed excellent catalytic activity for 4-NP reduction [120]. The system presents synergistic interaction and improves the activity of metal nanoparticles. Cu and Ag nanoparticles are evenly distributed on COFs, which provides active sites for 4-NP reduction. Cu/Ag-COF has high catalytic activity after 8 cycles, implying its high reusability. The pure COFs only acts as the catalyst carrier and had low catalytic activity, and. Besides, bimetallic Cu/Ag-COF presented the highest catalytic performance in 4-NP reduction, which was 2.28 times and 1.55 times that of Ag-COF and Cu-COF, respectively. The excellent performance of Cu/Ag-COF in the 4-NP reduction makes it have the potential to degrade 4-NP in water pollution treatment.

3.2. The applications of MPCM in MOR

Direct methanol fuel cells based on the electrocatalytic oxidation of methanol is one of the most promising energy conversion technologies due to its high effectiveness, simpler handling and delivery of liquid fuels, ease in operation and so on [154–157]. Electrocatalytic MOR as a vital reaction has drawn much attention [158–160]. The MOR including multi-step reaction path and different reaction intermediates. Formic acid is one of the intermediates, in addition to strong adsorption of CO and CO₂, which is the end product in addition to water [160,161]. However, the sluggish kinetics of the MOR suppresses its potential applications like the direct methanol fuel cells. Therefore, it is important to design efficient electrocatalysts to advance reaction kinetics and improve MOR catalytic activity. MPCM with abundant interface enable boosted MOR kinetics *via* the synergistic effect from different components [162,163]. For instance, Wang *et al.* have synthesized bimetallic NiCo-MOF through the assembly of 2,2'-bipyridine-5,5'-dicarboxylic acid with mixed Ni and Co acetates by one-pot method (Fig. 20) [164]. NiCo-MOF exhibited the best electrochemical MOR activity, which was ascribed to the synergistic interaction of Ni and Co. There are some factors that are beneficial for the enhancement of catalytic performance: (1) The high porosity is conducive to the diffusion of methanol; (2) The existed Ni²⁺ and Co²⁺ sites can synergistically improve the reaction kinetics, thus significantly improving the performance of electrocatalytic MOR. Specifically, NiCo-MOF displayed a high current density of 225 mA/cm² (at 1.6 V) in an alkaline electrolyte containing 0.5 mol/L methanol. Meanwhile, it also presented excellent long-term reaction stability.

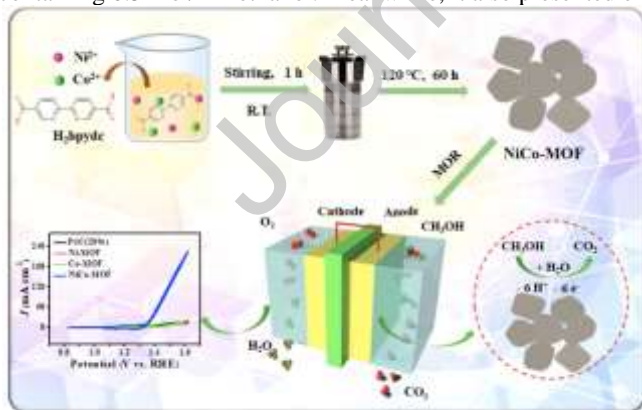


Fig. 20. Diagram of preparation of NiCo-MOF and its use as MOR electrocatalyst. Reproduced with permission [164]. Copyright 2021, Elsevier Inc.

4. Applications of MPCM in electrocatalytic reduction reaction

As the complementary half reaction of oxidation reaction in an electrolytic cell, electrocatalytic reduction reaction has comparable importance and serves as another main scope in the development of MPCM electrocatalysts [165–169]. In this section, we will review the applications of MPCM in HER, CO₂RR and ORR. The superiority of MPCM as advanced reduction electrocatalysts for energy conversion are described and discussed in detail.

4.1. The applications of MPCM in HER

H₂ is regarded as an ideal energy resource and promising substitute for fossil fuels [170,171]. Among various strategies for H₂ production, HER is regarded as an effective process due to its suitable manufacture and high product purity [172–176]. So far, the most effective electrocatalysts for HER are precious Pt-based materials yet they are still short in problems like high price or low reserve in earth [165,177–180]. Therefore, it is necessary to explore efficient catalysts to replace Pt-based catalysts and improve HER catalytic activity. During past years, MPCMs have exhibited high electrocatalytic activities in HER and a large number of interesting works have been reported [72,181]. The following section will discuss the recent development of MPCM in HER based on the classification from bimetallic MOFs and Tetra-metallic MOFs.

4.1.1. Bimetallic MOFs

Bimetallic MOFs like M_xNi_{1-x}-NKU-101 (M = Mn, Co, Cu, Zn) have been prepared by Zhang *et al.* using Ni-NKU-101 as the matrix (Fig. 21) [98]. The overpotential of Cu_{0.19}Ni_{0.81}-NKU-101 at 10 mA/cm² was 324 mV in 0.5 mol/L sulfuric acid electrolyte for HER. Interestingly, the ratio of Cu/Ni possessed apparent effect on the activity of Cu_xNi_{1-x}-NKU-101 electrocatalyst. This synergistic effect may be attributed to the following factors: (1) The binding of Cu and Ni on the surface of MOFs produced a suitable adsorption site that was beneficial for the hydrogen binding energy optimization; (2) The metal ratio of Cu and Ni can effectively change the ligand interaction and adjust the D-band position; (3) The spongy crystal surface generated by Cu²⁺ exchange greatly expanded the accessible active sites.

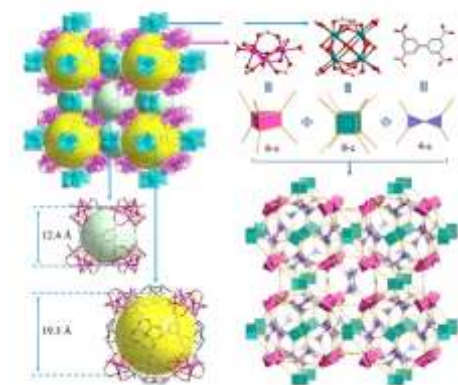


Fig. 21. Crystal structure of Ni-NKU-101. Reproduced with permission [98]. Copyright 2022, Wiley-VCH.

4.1.2. Tetra-metallic MOF

Besides, Zheng *et al.* *in-situ* grew a series of tetra-metallic MOF-74 on Ni foam (NF) [72]. It presented better electrocatalytic performance than bimetallic and trimetallic MOFs materials. FeCoMnNi-MOF-74/NF with multilayer hollow structure was prepared and applied as an efficient bi-functional electrocatalyst for water splitting. From the overpotential value of MOFs, it was observed that the multilayer hollow nanostructure was beneficial for the electrocatalytic process, providing sufficient active metal centers for FeCoMnNi-MOF-74/NF, making full use of the electrocatalyst, and having a synergistic effect of full mixing and dispersion. In 1 mol/L KOH, the overpotential of OER and HER is 250 and 108 mV for the current density of 50 and 10 mA/cm², and the Tafel slope is 41.28 and 72.89 mV/dec, respectively (Figs. 22a and b). Besides, as a bifunctional catalyst for water splitting, FeCoMnNi-MOF-74/NF requires a low cell voltage of 1.62 V to reach 10 mA/cm² current density. It is superior to other polymetallic-MOF-74 composites under the same conditions, and also exceeds the benchmark of commercially available precious metal catalysts. Additionally, In impedance test and long-term stability test, the material also has the advantages of low impedance and high stability (Figs. 22c and d).

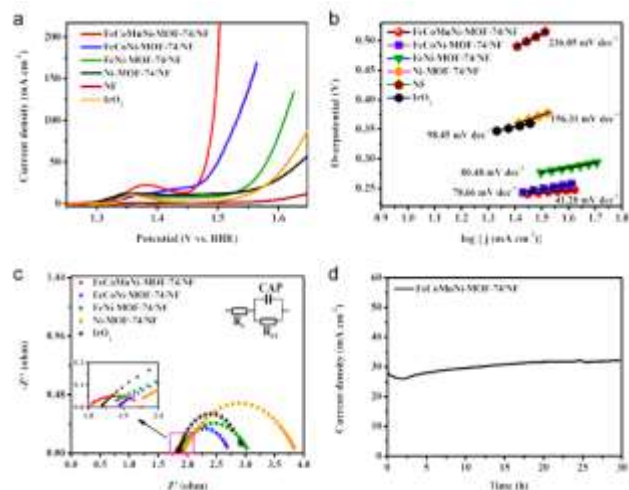


Fig. 22. Electrocatalytic performance of FeCoMnNi-MOF-74/NF. (a) LSV curves. (b) Tafel diagram. (c) Nyquist plots. (d) Chronoamperometric curve at 1.65 V. Reproduced with permission [72]. Copyright 2021, ACS.

4.2. The applications of MPCM in CO₂RR

Electrocatalytic CO₂RR has attracted much attention due to its ability of using clean energy to convert the greenhouse gas CO₂ into high value-added chemicals such as carbon monoxide, formic acid, ethylene, and ethanol [182–185]. However, the sluggish kinetics of CO₂ reduction with large energy barriers and competitive side reactions restrict its practical application [186–189]. Therefore, it is desired to develop efficient electrocatalysts to achieve high selectivity, high activity and low energy consumption. Specifically, MPCM shows much potential to be used as electrocatalysts in CO₂RR. For example, Huang *et al.* have reasonably designed and synthesized a new ultra-stable bimetallic phthalocyanine COFs (*i.e.*, CuPcF₈-CoPc-COF and CuPcF₈-CoNPc-COF) and explored its electrochemical CO₂ reduction performance and catalyst stability (Figs. 23a-c) [92]. Notably, the LSV curves showed that CuPcF₈-CoPc-COF has a smaller onset potentials of -0.4 V than that of CuPcF₈-CoNPc-COF (-0.42 V). Besides, CuPcF₈-CoNPc-COF displayed a FE_{CO} of 97% and an exceptionally high TOF of 2.87 s⁻¹, which is superior to CuPcF₈-CoPc-COF (FE_{CO}, 91%; TOF, 1.25 s⁻¹) and most COF-based electrocatalysts (Fig. 23d). The reasons for the high performance of CuPcF₈-CoNPc-COF can be ascribed to its larger pore size and stronger π - π stacking interaction that can facilitate the CO₂ capture and electron transfer for more efficient CO₂RR.

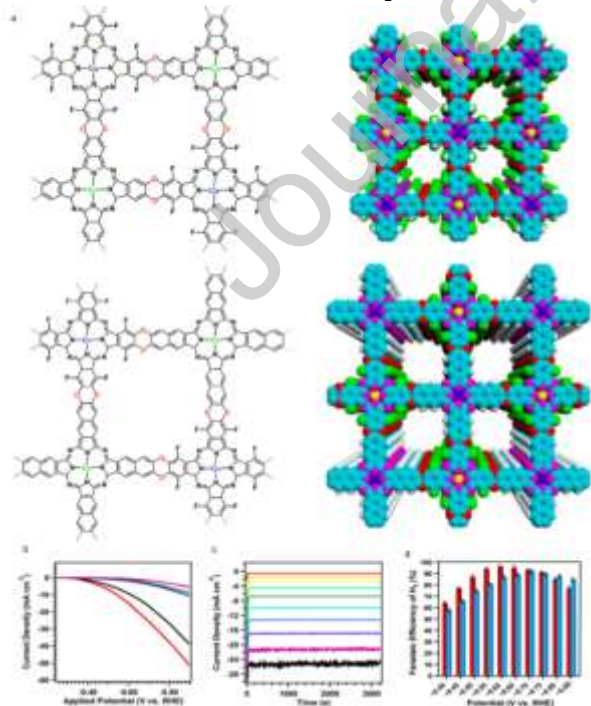


Fig. 23. Schematic illustration and electrocatalytic CO₂ reduction performance of CuPcF₈-CoPc-COF and CuPcF₈-CoNPc-COF. (a) Synthesis process. (b) LSV curves of CuPcF₈-CoPc-COF (black), CuPcF₈-CoNPc-COF (red). (c) I-t curves of CuPcF₈-CoNPc-COF at different potentials (from top to bottom: -0.35 V, -0.38 V, -0.41 V, -0.46 V, -0.50 V, -0.55 V, -0.59 V, -0.63 V, -0.67 V, -0.7 V). (d) FE_{CO} of CuPcF₈-CoPc-COF (blue) and CuPcF₈-CoNPc-COF (red). Reproduced with permission [92]. Copyright 2021, ACS.

Besides, Marinescu *et al.* synthesized a novel rhenium bipyridine COFs (*i.e.*, COF-Re_Co, COF-Re_Fe) with metallic porphyrins and bipyridinium units [89]. In this experiment, the authors also studied the electrocatalytic CO₂ reduction activity of COF-Re, COF-Re_Co and COF-Re_Fe in phosphate buffered aqueous solution with pH 7.2 and 0.5 mol/L KHCO₃. The result show that COF-Re_Co performed the highest activity for CO₂RR, achieving a FE_{CO} of 18%. The low selectivity for CO₂RR may be ascribed to a competitive relationship between the two metal centers as opposed to the desired synergistic relationship.

4.3. The applications of MPCM in ORR

ORR is an important cathodic reaction process for energy conversion in devices like metal-air batteries and fuel cells [190–193]. The four electron-reaction processes of ORR have the key intermediates, such as O₂*, OOH*, O*, and OH*. The reaction free energies of these reaction intermediates are crucial evaluation criteria for the ORR activities. The sluggish reaction kinetics and high overpotential of ORR in fuel cells lead to the inefficient conversion of chemical energy into electricity [194,195]. Therefore, it is crucial to design efficient electrocatalysts to selectively catalyze the ORR reactions. The following section will summarize the recent development of MPCM in ORR.

4.3.1. Bimetallic MOFs

Wang *et al.* used Fe and Co salts and tricarboxylic acids to synthesize a kind of MOFs (*i.e.*, MOFs (Fe/Co)) [196]. The high porosity is conducive to oxygen diffusion in catalysts and the utilization of catalytic sites, which is favorable for the improvement of OER and ORR. In the range of 0.35–0.55 V potential, ORR occurs mainly through dual electron pathway. When the potential scans more negative, ORR occurs through the four-electron and two-electron hybrid pathways, and gradually develops towards the four-electron pathway. In the range of 0.55–1.0 V potential, the number of electron transfer varies with the change of potential, indicating that the ORR is affected by the overpotential.

4.3.2. Bimetallic COFs

Sun *et al.* synthesized a multifunctional electrochemical catalyst bimetallic COFs (*i.e.*, Fe, Co-COF) and explored its ORR performance (Fig. 24a) [91]. The catalyst showed high electrocatalytic activity in ORR, with a positive half-wave potential (50 mV), a higher limiting diffusion current density, and a lower Tafel slope than that of Pt-C. In addition, the catalyst showed excellent electrochemical performance for HER, with overpotential of -0.26 V and -0.33 V at 10 mA/cm² in acidic and alkaline aqueous solutions, respectively (Figs. 24b–e). The excellent properties of COFs are due to the synergic structure effect: (1) Fe and Co in COFs facilitate the graphitization process and promote the formation of rich carbon layers around Fe and Co nanoparticles; (2) The carbon layers can protect the nanoparticles under alkaline conditions and improve their durability; (3) Compared with microporous structures, metal nanoparticles contribute to the formation of mesoporous structures and enhance the ion transport for the activity improvement of ORR and HER.

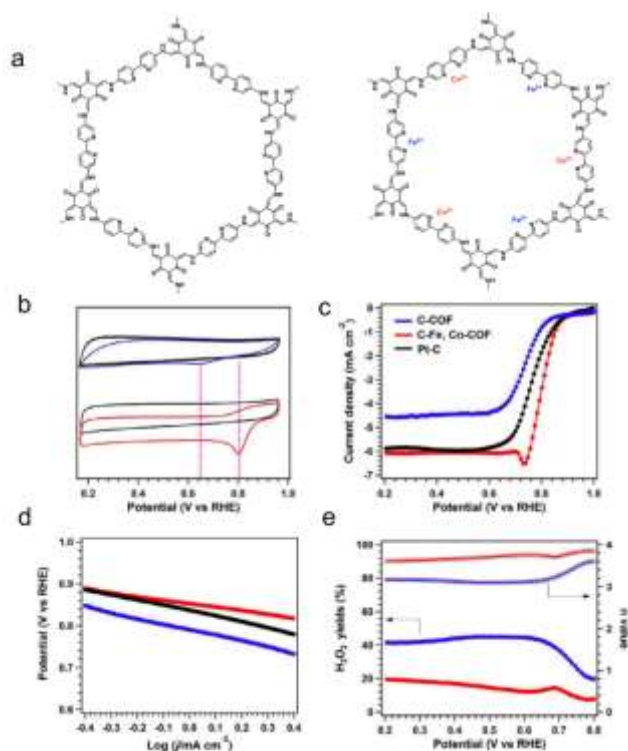


Fig. 24. Synthesis and electrocatalytic performance of the materials. (a) Synthesis of Fe, Co-COF. (b) CV curves. (c) RDE curves. (d) Tafel diagrams. (e) Number of transferred electrons and H_2O_2 yields. C-COF (blue) and C-Fe, Co-COF (red). Reproduced with permission [91]. Copyright 2018, European Chemical Societies Publishing.

5. Applications of MPCM in full electrolytic cell

In the above section, MPCM have exhibited much potential as the electrocatalysts for both electrocatalytic reduction and oxidation reactions. Henceforth, the MPCM might also serve as bifunctional catalyst to catalyze full electrolytic cell reaction. In this section, the full electrolytic cell reaction (*e.g.*, water splitting), a class of important catalysis reactions that can convert low-value substrates into more valuable products through the electron and proton transfer processes [144,145,197], is reviewed sequentially. The superiority of MPCM as advanced electrocatalysts for energy conversion is described and discussed in detail.

Some bimetallic MOFs can simultaneously show excellent performance in HER and OER, acting as a bi-functional catalyst for water splitting. For instance, Vishnu *et al.* reported that rCoFe-PBA can produce hydrogen in alkaline water [197]. The overpotential of rCoFe-PBA-coated foam Ni electrode was 311 mV (OER) and 100 mV (HER) at 10 mA/cm^2 , which was much lower than that of IrO_2 (381 mV) and close to Pt/C (36 mV). The turnover frequency (TOF) was calculated to be 0.22 s^{-1} (OER), which was five times larger than that of IrO_2 (0.040 s^{-1}). Meanwhile, the TOF for HER was 0.26 s^{-1} , which was ten times larger than that of Pt/C (0.025 s^{-1}). Under the test condition of solar electrolysis, the overpotential of rCoFe-PBA at 1 mol/L KOH was 411 mV, and the durability exceeded 180 h.

Furthermore, Du *et al.* reported an ultra-low ruthenium-doped Ni-Co-MOF hollow porous nanospheres (Ru@NiCo-MOF HPNs) [119]. The obtained $\text{Ru@NiCo-MOF-4 HPNs}$ exhibit a three-dimensional, uniform hollow spherical structure composed of many layered nanosheets. The addition of Ru to NiCo-MOF HPNs can stabilize OER activity for at least 39 h. Besides, due to the high porosity and large surface area of MOFs and the electronic properties optimized by Ru doping, the optimized $\text{Ru@NiCo-MOF-4 HPNs}$ (13.5 at% Ru doping) presented the highest OER activity with high mass activity (310 mA/mg) at 284 mV overpotential. In addition, the Ru@NiCo-MOF-4 based two-electrode cells (anode, Ru@NiCo-MOF-4 and cathode, commercial Pt/C) also displayed excellent electrochemical water splitting property (cell potential of 1.57 V at 10 mA/cm^2) (Figs. 25a and b). Specifically, Ru@NiCo-MOF HPNs showed an overpotential of 284 mV and a Tafel slope of 78.8 mV/dec at 10 mA/cm^2 in alkaline electrolyte (Figs. 25c and d). They performed EIS analyses on Ru@NiCo-MOF-4 and Ni-Co-MOF to study the charge transfer property in the water decomposition reaction. It is obvious that the semicircle of Ni-Co-MOF was wider than Ru@NiCo-MOF-4 and was positively correlated with the value of charge transfer resistance (R_{ct}), implying the electron transfer at the interface is increased after doping with ultra-low ruthenium, which corresponds to the increase of OER and HER activity.

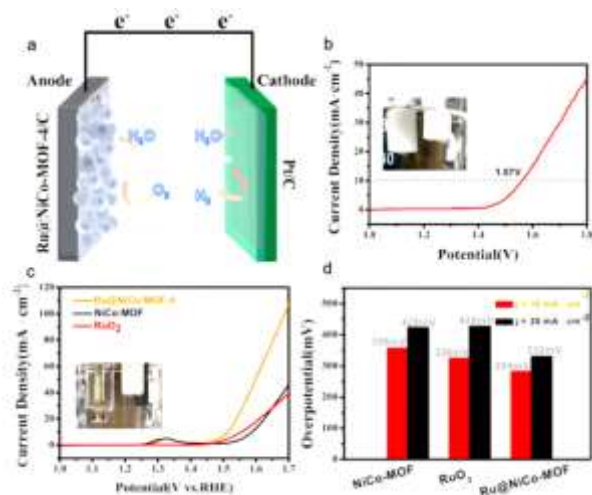


Fig. 25. Electrochemical performance of materials. (a) Schematic illustration of water splitting. (b) LSV curve of water splitting. (c) LSV curves. (d) Overpotential required for Ru@NiCo-MOF-4, NiCo-MOF, and commercial RuO₂ to achieve 10 mA/cm² and 30 mA/cm². Reproduced with permission [119]. Copyright 2021, ACS.

6. Perspective

Based on above-mentioned content, we have summarized the applications of MPCM in electrocatalytic yet there are still some important issues need to be summarized and discussed. Owing to the advantages of these materials, they generally display high porosity, multi-metal active sites, well-tuned functions, and pre-designable structures, *etc.*, serving as desired platforms for electrocatalytic reactions like HER, OER and CO₂RR *ect*. For MPCM, the imparted two or more metal sites in their structures offer more opportunity in designing multifunctionality or well-tuned metal sites for a wider range of applications. Specifically, MPCM may deliver superior property over none or single metal porous crystalline materials by providing complexity and introducing multifunctionality derived from the integration of different metal sites in the structures. MPCM have attracted much attention in different electrocatalytic reactions owing to the following advantages: (1) The introduction of multi-metal might affect the disorder of the lattice to result in more unique properties; (2) The imparted accessible metal sites in the porous structure would optimize the electron cloud density to enhance the catalytic activity; (3) The existed three or more different metal sites in a catalyst might lead to high-entropy alike state in MPCM that can endow diversified microenvironments to boost the performance. However, as a result of the possibly existed synergistic effect that comes from the interaction among two or more metal sites, MPCM might exhibit much more potential with better performance when compared with none or single metal porous crystalline materials in electrocatalysis.

However, there are still some existed bottlenecks for the applications of MPCM in electrocatalysis: (1) A systematic study for the modulation of conditions and limitations of strategies that is controlled by thermodynamics or kinetics is still challenging; (2) The precise definition of the location of multi-metal sites is essential yet still hard for further applications; (3) The relationship of structural features and electrocatalytic activity are crucial for identifying the active sites and mechanistic study; (4) The low-cost and scalable MPCM systems is meaningful for the potentially large-scale industrial production and practical applications.

To address these bottlenecks, potential methods of these materials might be noted as follows. For the preparation of MPCM, we need to explore more facile and readily available methods based on the one-pot and post-synthetic modification ones that can systematically consider the overall cost, efficiency and possibility of mass production. For the characterizations MPCM, more advanced techniques need to be explored to define the actuate multi-metal sites, which is also vital for the mechanistic study to reveal their possible interaction or synergistic effect of these metal sites. For the stability of MPCM, we need to design explore more stable porous frameworks through the specific selection of structure struts, which would be much beneficial for the post-synthetic treatment or harsh condition electrocatalysis. At present, most of the applications in electrocatalysis are mostly limited to OER or HER, more advanced and valuable reduction-type reactions is needed to maximize the advantages of MPCM. Meanwhile, a more depth understanding of inherent structure-property relationship is extremely important for the directional design of MPCM in electrocatalysis applications.

7. Conclusion

In this review, the preparation strategy, structure, composition, electrocatalytic performance, and reaction mechanism of MPCM were analyzed. It provides guidance and powerful inspiration for the potential application of this material in energy related fields. This paper also reviews the major challenges, solutions and potential development trends of MPCM as advanced electrocatalysts for energy storage and conversion, and further explores the innovation of these materials in energy storage and conversion. Besides, the challenges faced by MPCM are summarized and the relevant solutions and prospects are proposed. We anticipate this review will

provide a new perspective or guide to readers' deep understanding of this field, and promote the application and development of MPCM in energy conversion to expand the limitations of current electrocatalysis technologies.

Acknowledgments

This work was financially supported by The National Key R&D Program of China (No. 2023YFA1507204), The National Natural Science Foundation of China (Nos. 22171139, 22225109, 22309054, 22071109, 22371080, 21775048), Natural Science Foundation of Guangdong Province (No. 2023B1515020076), China Postdoctoral Science Foundation (No. 2023M731154), China National Postdoctoral Program for Innovative Talents (No. BX20220116).

References

- [1] Materials Design and Discovery Group, H.K. Chae, D.Y. Siberio-Pérez, et al., *Nature* 427 (2004) 523–527.
- [2] Y. Zheng, Y. Jiao, M. Jaroniec, S.Z. Qiao, *Angew. Chem. Int. Ed.* 54 (2015) 52–65.
- [3] D. Yuan, D. Zhao, D. Sun, H.C. Zhou, *Angew. Chem. Int. Ed.* 49 (2010) 5357–5361.
- [4] A.P. Cote, A.I. Benin, N.W. Ockwig, et al., *Science* 310 (2005) 1166–1170.
- [5] C. Guo, J. Zhou, Y. Chen, et al., *Angew. Chem. Int. Ed.* 61 (2022) e202210871.
- [6] J. Chang, Q. Li, J. Shi, et al., *Angew. Chem. Int. Ed.* 62 (2023) e202218868.
- [7] L.Z. Dong, Y.F. Lu, R. Wang, et al., *Nano Res.* 15 (2022) 10185–10193.
- [8] Y. Wang, H. Ding, S. Sun, et al., *Angew. Chem. Int. Ed.* 61 (2022) e202212162.
- [9] X. Yao, C. Guo, C. Song, et al., *Adv. Mater.* 35 (2023) 2208846.
- [10] Y. Wang, H. Ding, X. Ma, et al., *Angew. Chem. Int. Ed.* 61 (2022) e202114648.
- [11] C. Hou, L. Zou, Q. Xu, *Adv. Mater.* 31 (2019) 1904689.
- [12] C.S. Feng, T.W. Lu, T.L. Wang, et al., *Acta Metall. Sin. Engl. Lett.* 34 (2021) 1537–1545.
- [13] L. Wei, H.E. Karahan, S. Zhai, et al., *Adv. Mater.* 29 (2017) 1701410.
- [14] J. Song, C. Zhu, B.Z. Xu, et al., *Adv. Energy Mater.* 7 (2017) 1601555.
- [15] X. Han, C. Jiang, B. Hou, et al., *J. Am. Chem. Soc.* 146 (2024) 6733–6743.
- [16] C. Li, Z. Qiu, H. Sun, Y. Yang, C.P. Li, *Chin. J. Struct. Chem.* 41 (2022) 2211084–2211099.
- [17] S. Ruidas, B. Mohanty, P. Bhanja, et al., *ChemSusChem* 14 (2021) 5057–5064.
- [18] X. Huang, C. Sun, X. Feng, *Sci. China Chem.* 63 (2020) 1367–1390.
- [19] J. Pang, R.G. Mendes, A. Bachmatiuk, et al., *Chem. Soc. Rev.* 48 (2019) 72–133.
- [20] H. Sun, Z. Yan, F. Liu, et al., *Adv. Mater.* 32 (2020) 1806326.
- [21] J. Liu, Y. Gao, Y. Wei, et al., *Chem. Commun.* 56 (2020) 4228–4231.
- [22] Y. Hu, W. Liu, K. Jiang, et al., *Inorg. Chem. Front.* 7 (2020) 4461–4468.
- [23] Q. Gan, B. Liu, K. Zhao, Z. He, S. Liu, *Electrochimica Acta* 279 (2018) 152–160.
- [24] J. Huang, H. Sheng, R.D. Ross, et al., *Nat. Commun.* 12 (2021) 3036.
- [25] L. Wan, P. Wang, *Int. J. Hydrog. Energy* 46 (2021) 8356–8376.
- [26] G. Lee, W. Na, J. Kim, S. Lee, J. Jang, *J. Mater. Chem. A* 7 (2019) 17637–17647.
- [27] S. Anantharaj, K. Karthick, S. Kundu, *Mater. Today Energy* 6 (2017) 1–26.
- [28] M. Gong, Y. Li, H. Wang, et al., *J. Am. Chem. Soc.* 135 (2013) 8452–8455.
- [29] C.C.L. McCrory, S. Jung, J.C. Peters, T.F. Jaramillo, *J. Am. Chem. Soc.* 135 (2013) 16977–16987.
- [30] D. Yang, B.C. Gates, *ACS Catal.* 9 (2019) 1779–1798.
- [31] Z.W. Seh, J. Kibsgaard, C.F. Dickens, et al., *Science* 355 (2017) <https://doi.org/10.1126/science.aad4998>.
- [32] X.F. Lu, L. Yu, X.W. (David) Lou, *Sci. Adv.* 5 (2019) eaav6009.
- [33] W.Q. Zhou, B.J. Xi, X.W. Chang, et al., *Molecules* 27 (2022) 2113.
- [34] X. Zhang, H. Pan, Y. Jia, et al., *J. Colloid Interf. Sci.* 623 (2022) 552–560.
- [35] Q. Wang, Z. Liu, H. Zhao, et al., *J. Mater. Chem. A* 6 (2018) 18720–18727.
- [36] Z. Gao, Y. Lai, L. Zhang, et al., *J. Chem. Educ.* 98 (2021) 3341–3347.
- [37] J. Yang, X. Wang, Y. Qu, et al., *Adv. Energy Mater.* 10 (2020) 2001709.
- [38] J. Li, M. Zhang, H. Zang, et al., *ChemCatChem* 11 (2019) 4998–5012.
- [39] P. Zhang, L. Li, D. Nordlund, et al., *Nat. Commun.* 9 (2018) 381.
- [40] X. Zhao, X. Li, Y. Yan, et al., *Appl. Catal. B: Environ.* 236 (2018) 569–575.
- [41] Z. Kang, H. Guo, J. Wu, et al., *Adv. Funct. Mater.* 29 (2019) 1807031.
- [42] M.B. Stevens, L.J. Enman, E.H. Korkus, et al., *Nano Res.* 12 (2019) 2288–2295.
- [43] Z. Lu, L. Qian, Y. Tian, et al., *Chem. Commun.* 52 (2016) 908–911.
- [44] C. Worch, F. Kettner, D. Laessig, et al., *Catal. Commun.* 44 (2014) 46–49.
- [45] V. Rubio-Giménez, J.C. Waerenborgh, J.M. Clemente-Juan, C. Martí-Gastaldo, *Chem. Mater.* 29 (2017) 6181–6185.
- [46] S. Wang, W. Huo, F. Fang, et al., *Chem. Eng. J.* 429 (2022) 132410.
- [47] J.K. Sun, Q. Xu, *ENERGY Environ. Sci.* 7 (2014) 2071–2100.
- [48] C. Castillo-Blas, F. Gandara, *Isr. J. Chem.* 58 (2018) 1036–1043.
- [49] M.Y. Masoomi, A. Morsali, A. Dhakshinamoorthy, H. Garcia, *Angew. Chem. Int. Ed.* 58 (2019) 15188–15205.
- [50] J.S. Kim, B. Kim, H. Kim, K. Kang, *Adv. Energy Mater.* 8 (2018) 1702774.
- [51] L.J. Wang, H. Deng, H. Furukawa, et al., *Inorg. Chem.* 53 (2014) 5881–5883.
- [52] Y. Wang, S. Zhao, Y. Zhu, et al., *iScience* 23 (2020) 100761.
- [53] S. Qiu, M. Xue, G. Zhu, *Chem. Soc. Rev.* 43 (2014) 6116–6140.
- [54] Y.Z. Chen, R. Zhang, L. Jiao, H.L. Jiang, *Coord. Chem. Rev.* 362 (2018) 1–23.
- [55] A. Shafiei, *Met. Mater. Int.* 27 (2021) 127–138.
- [56] L. Han, X.Y. Yu, X.W.D. Lou, *Adv. Mater.* 28 (2016) 4601–4605.
- [57] Y. Zhai, X. Ren, B. Wang, S. (Frank) Liu, *Adv. Funct. Mater.* 32 (2022) 2207536.
- [58] T.Y. Luo, C. Liu, X.Y. Gan, et al., *J. Am. Chem. Soc.* 141 (2019) 2161–2168.
- [59] O.S. Bushuyev, P. De Luna, C. T. Dinh, et al., *Joule* 2 (2018) 825–832.
- [60] H. Rao, L.C.S. Chmidt, J. Bonin, M. Robert, *Nature* 548 (2017) 74.
- [61] D. Ren, B.S.H. Ang, B.S. Yeo, *ACS Catal.* 6 (2016) 8239–8247.
- [62] Y. Xu, B. Zhang, *ChemElectroChem* 6 (2019) 3214–3226.

- [63] X. Huang, Q. Shen, J. Liu, N. Yang, G. Zhao, *Energy Environ. Sci.* 9 (2016) 3161–3171.
- [64] S. Verma, S. Lu, P.J.A. Kenis, *Nat. Energy* 4 (2019) 466–474.
- [65] X. Deng, M. Li, Y. Fan, et al., *Appl. Catal. B: Environ.* 278 (2020) 119339.
- [66] M. Lu, M. Zhang, J. Liu, et al., *Angew. Chem. Int. Ed.* 61 (2022) e202200003.
- [67] Z. Mi, T. Zhou, W. Weng, et al., *Angew. Chem. Int. Ed.* 60 (2021) 9642–9649.
- [68] D. S. Raja, C.L. Huang, Y.A. Chen, Y. Choi, S.Y. Lu, *Appl. Catal. B: Environ.* 279 (2020) 119375.
- [69] Z. Chen, D. Liu, Y. Gao, et al., *Sci. China Mater.* 65 (2022) 1217–1224.
- [70] D.X. Yang, P.F. Wang, H.Y. Liu, et al., *J. Solid State Chem.* 309 (2022) 122947.
- [71] Z. Li, S. Deng, H. Yu, et al., *J. Mater. Chem. A* 10 (2022) 4230–4241.
- [72] M. Zhang, W. Xu, T. Li, H. Zhu, Y. Zheng, *Inorg. Chem.* 59 (2020) 15467–15477.
- [73] Y. Yao, Z. Ma, Y. Dou, et al., *Chem. Eur. J.* 28 (2022) e202104288.
- [74] J.M. Saveant, C. Tard, *J. Am. Chem. Soc.* 138 (2016) 1017–1021.
- [75] Y. Li, K. Zuo, T. Gao, et al., *RSC Adv.* 12 (2022) 4874–4882.
- [76] R. Losantos, D. Sampedro, *Molecules* 26 (2021) 3796.
- [77] S.P.S. Fernandes, A. Mellah, P. Kovar, et al., *Molecules* 25 (2020) 3132.
- [78] I. Bar-Nahum, A. Khenkin, R. Neumann, *J. Am. Chem. Soc.* 126 (2004) 10236–10237.
- [79] M. Jiang, X. Meng, W. Zhang, et al., *Electrochem. Commun.* 126 (2021) 107004.
- [80] Y. Kim, Y.W. Lee, M. Kim, S.W. Han, *Chem. Eur. J.* 20 (2014) 7901–7905.
- [81] P. Guo, Q. Wang, Y. Sang, et al., *Sci. Adv. Mater.* 8 (2016) 1345–1353.
- [82] M. Tang, W. Chen, S. Luo, et al., *J. Mater. Chem. A* 9 (2021) 9602–9608.
- [83] K. Wu, K. Sun, S. Liu, et al., *Nano Energy* 80 (2021) 105467.
- [84] A. Begum, P.G. Pickup, *Electrochem. Commun.* 9 (2007) 2525–2528.
- [85] M. Jia, L. Shen, G. Tian, et al., *Chem. Asian J.* 17 (2022) e202200449.
- [86] L. Gloag, T.M. Benedetti, S. Cheong, et al., *Angew. Chem. Int. Ed.* 57 (2018) 10241–10245.
- [87] Y. Wang, J. Kim, *Electroanalysis* 31 (2019) 1026–1033.
- [88] Z. Lu, C. Wei, X. Liu, et al., *Mater. Chem. Front.* 5 (2021) 6092–6100.
- [89] E.M. Johnson, R. Haiges, S.C. Marinescu, *ACS Appl. Mater. Interfaces* 10 (2018) 37919–37927.
- [90] X. Wang, H. Xiao, A. Li, et al., *J. Am. Chem. Soc.* 140 (2018) 15336–15341.
- [91] D. Wu, Q. Xu, J. Qian, X. Li, Y. Sun, *Chem. Eur. J.* 25 (2019) 3105–3111.
- [92] Y. Yue, P. Cai, K. Xu, et al., *J. Am. Chem. Soc.* 143 (2021) 18052–18060.
- [93] W. Zhou, Z. Xue, Q. Liu, et al., *ChemSusChem* 13 (2020) 5647–5653.
- [94] W. Xu, H. Chen, K. Jie, et al., *Angew. Chem. Int. Ed.* 58 (2019) 5018–5022.
- [95] X. Zhao, Z. Xue, W. Chen, et al., *J. Mater. Chem. A* 7 (2019) 26238–26242.
- [96] J. Cui, J. Liu, C. Wang, et al., *Electrochim. Acta* 334 (2020) 135577.
- [97] S. Zhao, C. Tan, C.T. He, et al., *Nat. Energy* 5 (2020) 881–890.
- [98] R. Zhang, L. Lu, Z. Chen, et al., *Chem. Eur. J.* 28 (2022) e202200401.
- [99] G. Zhan, H.C. Zeng, *Chem. Commun.* 53 (2017) 72–81.
- [100] R. Francke, B. Schille, M. Roemelt, *Chem. Rev.* 118 (2018) 4631–4701.
- [101] J. Xing, K. Guo, Z. Zou, et al., *Chem. Commun.* 54 (2018) 7046–7049.
- [102] Y. Wang, M. Liu, G. Gao, et al., *Angew. Chem. Int. Ed.* 60 (2021) 21952–21958.
- [103] Q. Li, Z.M. Wang, Y. Chen, et al., *J. Mater. Chem. A* 10 (2022) 25356–25362.
- [104] W. Zhou, L. Gao, Y. Zhang, T. Hu, *Int. J. Hydrog. Energy* 46 (2021) 27128–27137.
- [105] R. Mehek, N. Iqbal, T. Noor, et al., *Electrochim. Acta* 255 (2017) 195–204.
- [106] C. Wang, J. Kim, J. Tang, et al., *Chem* 6 (2020) 19–40.
- [107] M. Kang, D.W. Kang, C.S. Hong, *Dalton Trans.* 48 (2019) 2263–2270.
- [108] T. Chen, D. Zhao, *Coord. Chem. Rev.* 491 (2023) 215259.
- [109] M. Kandiah, S. Usseglio, S. Svelle, et al., *J. Mater. Chem.* 20 (2010) 9848–9851.
- [110] B. Slater, S.O. Wong, A. Duckworth, et al., *Chem. Commun.* 55 (2019) 7319–7322.
- [111] M. Soleiman-Beigi, I. Yavari, F. Sadeghizadeh, *RSC Adv.* 5 (2015) 87564–87570.
- [112] Y. Duan, F. Ye, Y. Huang, et al., *Chem. Commun.* 54 (2018) 5377–5380.
- [113] Y. Wang, Y. Lu, Z. Li, et al., *Chem. Commun.* 57 (2021) 8933–8936.
- [114] L. Wang, W. Yang, Y. Li, et al., *Chem. Commun.* 50 (2014) 11653–11656.
- [115] S.H. Doan, C.B. Tran, A.N. Cao, N.T.H. Le, N.T.S. Phan, *Catal. Lett.* 149 (2019) 2053–2063.
- [116] P. Puthiaraj, A. Ramu, K. Pitchumani, *Asian J. Org. Chem.* 3 (2014) 784–791.
- [117] H. V. Dang, H. T. B. Le, L. T. B. Tran, et al., *RSC Adv.* 8 (2018) 31455–31464.
- [118] T. He, X.J. Kong, J. Zhou, et al., *J. Am. Chem. Soc.* 143 (2021) 9901–9911.
- [119] D. Liu, H. Xu, C. Wang, et al., *Inorg. Chem.* 60 (2021) 5882–5889.
- [120] Z. Wu, J. Zhu, W. Wen, X. Zhang, S. Wang, *J. Solid State Chem.* 311 (2022) 123116.
- [121] Y. Zhou, R. Abazari, J. Chen, et al., *Coord. Chem. Rev.* 451 (2022) 214264.
- [122] U. Khan, A. Nairan, J. Gao, Q. Zhang, *Small Struct.* 4 (2023) 2200109.
- [123] A. Radwan, H. Jin, D. He, S. Mu, *Nano-Micro Lett.* 13 (2021) 132.
- [124] X. Wang, Y. Feng, P. Dong, J. Huang, *Front. Chem.* 7 (2019) <https://doi.org/10.3389/fchem.2019.00671>.
- [125] H.F. Wang, C. Tang, Q. Zhang, *Adv. Funct. Mater.* 28 (2018) 1803329.
- [126] K. Zhang, R. Zou, *Small* 17 (2021) 2100129.
- [127] T. Tang, S. Li, J. Sun, Z. Wang, J. Guan, *Nano Res.* 15 (2022) 8714–8750.
- [128] J. Zhang, Z. Cui, J. Liu, et al., *Front. Phys.* 18 (2023) 13603.
- [129] M.I. James, M. Harb, *J. Energy Chem.* 56 (2021) 299–342.
- [130] S. Li, Y. Gao, N. Li, et al., *Energy Environ. Sci.* 14 (2021) 1897–1927.
- [131] B. Zhou, R. Gao, J.J. Zou, H. Yang, *Small* 18 (2022) 2202336.
- [132] H. Ding, H. Liu, W. Chu, C. Wu, Y. Xie, *Chem. Rev.* 121 (2021) 13174–13212.
- [133] J. Wang, M. Zhang, J. Li, et al., *Dalton Trans.* 49 (2020) 14290–14296.
- [134] L. Ai, Y. Luo, W. Huang, Y. Tian, J. Jiang, *Int. J. Hydrog. Energy* 47 (2022) 12893–12902.
- [135] K. Ge, S. Sun, Y. Zhao, et al., *Angew. Chem. Int. Ed.* 60 (2021) 12097–12102.

- [136] F. Sun, G. Wang, Y. Ding, et al., *Adv. Energy Mater.* 8 (2018) 1800584.
- [137] J. Zhang, L. Jin, P. Gu, et al., *ACS Appl. Nano Mater.* 4 (2021) 12407–12414.
- [138] X. Su, Y. Wang, J. Zhou, et al., *J. Am. Chem. Soc.* 140 (2018) 11286–11292.
- [139] Y. Fu, L. Xu, H. Shen, et al., *Chem. Eng. J.* 299 (2016) 135–141.
- [140] J. Li, W. Huang, M. Wang, et al., *ACS Energy Lett.* 4 (2019) 285–292.
- [141] X.L. Wang, L.Z. Dong, M. Qiao, et al., *Angew. Chem. Int. Ed.* 57 (2018) 9660–9664.
- [142] L. Huang, G. Gao, H. Zhang, et al., *Nano Energy* 68 (2020) 104296.
- [143] Y. Jiao, J. Pei, D. Chen, et al., *J. Mater. Chem. A* 5 (2017) 1094–1102.
- [144] M. Aghazadeh, H.F. Rad, *J. Energy Storage* 53 (2022) 105194.
- [145] M. Aghazadeh, H. Foratirad, *Mater. Lett.* 313 (2022) 131804.
- [146] S. He, Z. Li, J. Wang, *J. Solid State Chem.* 307 (2022) 122726.
- [147] S. Sun, M. Huang, P. Wang, M. Lu, *J. Electrochem. Soc.* 166 (2019) A1799–A1805.
- [148] Y. Shan, L. Chen, H. Pang, Q. Xu, *Small Struct.* 2 (2021) 2000078.
- [149] X.Y. Yu, Y. Feng, B. Guan, X.W. (David) Lou, U. Paik, *Energy Environ. Sci.* 9 (2016) 1246–1250.
- [150] F.L. Li, Q. Shao, X. Huang, J.P. Lang, *Angew. Chem. Int. Ed.* 57 (2018) 1888–1892.
- [151] S.S. Sankar, K. Manjula, G. Keerthana, B. Ramesh Babu, S. Kundu, *Cryst. Growth Des.* 21 (2021) 1800–1809.
- [152] S. Xu, M. Li, H. Wang, et al., *J. Phys. Chem. C* 126 (2022) 14094–14102.
- [153] X. Zuo, K. Chang, J. Zhao, et al., *J. Mater. Chem. A* 4 (2016) 51–58.
- [154] L. Zhang, M.J. Liu, D.Y. Zhu, et al., *Nat. Commun.* 15 (2024) 3409.
- [155] W. Li, D. Wang, Y. Zhang, et al., *Adv. Mater.* 32 (2020) 1907879.
- [156] D. Zhao, Z. Zhuang, X. Cao, et al., *Chem. Soc. Rev.* 49 (2020) 2215–2264.
- [157] N. Ramaswamy, S. Mukerjee, *Chem. Rev.* 119 (2019) 11945–11979.
- [158] Q. Wang, D. Astruc, *Chem. Rev.* 120 (2020) 1438–1511.
- [159] J. Kim, H.E. Kim, H. Lee, *ChemSusChem* 11 (2018) 104–113.
- [160] H. Niu, C. Xia, L. Huang, et al., *Chin. J. Catal.* 43 (2022) 1459–1472.
- [161] Y. Yang, M. Luo, W. Zhang, et al., *Chem* 4 (2018) 2054–2083.
- [162] Y. Yan, J. Miao, Z. Yang, et al., *Chem. Soc. Rev.* 44 (2015) 3295–3346.
- [163] X. Ren, Q. Lv, L. Liu, et al., *Sustain. Energy Fuels* 4 (2020) 15–30.
- [164] M. Wang, C. Wang, L. Zhu, et al., *Appl. Catal. Gen.* 619 (2021) 118159.
- [165] F. Gao, Y. Zhang, Z. Wu, H. You, Y. Du, *Coord. Chem. Rev.* 436 (2021) 213825.
- [166] Z. Pu, T. Liu, I.S. Amiinu, et al., *Adv. Funct. Mater.* 30 (2020) 2004009.
- [167] S. Li, E. Li, X. An, et al., *Nanoscale* 13 (2021) 12788–12817.
- [168] C.C. Weng, J.T. Ren, Z.Y. Yuan, *ChemSusChem* 13 (2020) 3357–3375.
- [169] Y. Zheng, Y. Jiao, A. Vasilieff, S.Z. Qiao, *Angew. Chem. Int. Ed.* 57 (2018) 7568–7579.
- [170] S.K. Saxena, V. Drozd, A. Durygin, *Int. J. Hydrog. Energy* 33 (2008) 3625–3631.
- [171] A. Steinfeld, *Fuel Cell World Proc.* (2002) 356–366.
- [172] S.M. Thalluri, L. Bai, C. Lv, et al., *Adv. Sci.* 7 (2020) 1902102.
- [173] P. Zhou, J. Lv, X. Huang, Y. Lu, G. Wang, *Coord. Chem. Rev.* 478 (2023) 214969.
- [174] S. Anantharaj, S. Noda, V.R. Jothi, et al., *Angew. Chem. Int. Ed.* 60 (2021) 18981–19006.
- [175] Y. Cao, *ACS Nano* 15 (2021) 11014–11039.
- [176] C. Wei, R.R. Rao, J. Peng, et al., *Adv. Mater.* 31 (2019) 1806296.
- [177] Z. Pu, I.S. Amiinu, R. Cheng, et al., *Nano-Micro Lett.* 12 (2020) 21.
- [178] L. Zou, Y.S. Wei, C.C. Hou, C. Li, Q. Xu, *Small* 17 (2021) 2004809.
- [179] P. Chen, J. Ye, H. Wang, L. Ouyang, M. Zhu, *J. Alloy. Compd.* 883 (2021) 160833.
- [180] Z.X. Wei, Y.T. Zhu, J.Y. Liu, et al., *Rare Met.* 40 (2021) 767–789.
- [181] L. Wang, L. Ren, X. Wang, et al., *ACS Appl. Mater. Interfaces* 10 (2018) 4750–4756.
- [182] X.B. Xu, D.F. Xiao, Y.G. Gao, et al., *ACS Appl. Mater. Interfaces* 16 (2024) 16243–16252.
- [183] Y. Pan, R. Abazari, Y. Wu, J. Gao, Q. Zhang, *Electrochem. Commun.* 126 (2021) 107024.
- [184] S. Zhang, Q. Fan, R. Xia, T.J. Meyer, *Acc. Chem. Res.* 53 (2020) 255–264.
- [185] M.G. Kibria, J.P. Edwards, C.M. Gabardo, et al., *Adv. Mater.* 31 (2019) 1807166.
- [186] X. Song, L. Xu, X. Sun, B. Han, *Sci. Chin. Chem.* 66 (2023) 315–323.
- [187] L. Lu, H. Zheng, Y. Li, Y. Zhou, B. Fang, *Chem. Eng. J.* 451 (2023) 138668.
- [188] S. Huang, K. Chen, T.T. Li, *Coord. Chem. Rev.* 464 (2022) 214563.
- [189] S.C. Sun, B. Peng, Y. Song, et al., *ACS Appl. Mater. Interfaces* 15 (2023) 12957–12966.
- [190] W.J.M. Kort-Kamp, M. Ferrandon, X. Wang, et al., *J. Power Sources* 559 (2023) 232583.
- [191] D. Alba-Molina, A.R. Puente Santiago, J.J. Giner-Casares, et al., *J. Phys. Chem. C* 123 (2019) 9807–9812.
- [192] G.R. Dillip, G.K. Kiran, A. Bharti, et al., *ACS Appl. Energy Mater.* 5 (2022) 13635–13644.
- [193] X. Ge, F.W.T. Goh, B. Li, et al., *Nanoscale* 7 (2015) 9046–9054.
- [194] S.K. Singh, K. Takeyasu, J. Nakamura, *Adv. Mater.* 31 (2019) 1804297.
- [195] X. Tian, X.F. Lu, B.Y. Xia, X.W. (David) Lou, *Joule* 4 (2020) 45–68.
- [196] H. Wang, F. Yin, G. Li, B. Chen, Z. Wang, *Int. J. Hydrog. Energy* 39 (2014) 16179–16186.
- [197] B. Vishnu, S. Mathi, S. Sriram, J. Jayabharathi, *ChemistrySelect* 7 (2022) e202201682.

Author Biographies



Ming Yue received her B. Eng. degree at East China University of Science and Technology in 2021, and is now studying for a postgraduate degree at South China Normal University under the supervision of Prof. Ya-Qian Lan and Prof. Yifa Chen. Her research interest focuses on the design and synthesis of crystalline porous materials (MOF- and COF-based composites) for energy conversion.



Yi-Rong Wang received her M.S. degree (2019) and Ph.D. degrees (2022) from Nanjing Normal University under the supervision of Prof. Ya-Qian Lan. Since 2022, she has carried out postdoctoral research at South China Normal University with Prof. Ya-Qian Lan. Her current research focuses on the synthesis of crystalline porous materials (MOF- and COF-based composites) and their applications in energy storage and conversion.

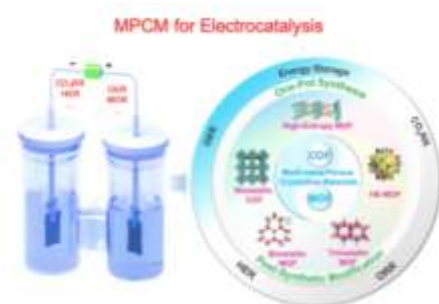


Xiao-Gang Hu received his Ph.D. degree (2008) from the School of Chemistry and Chemical Engineering, Sun Yat-sen University. He joined the Analytical Chemistry Committee of Guangdong Chemical Society and the Chromatography Committee of Guangdong Analytical Testing Association. He joined South China Normal University (SCNU, China) in 2001, and is now a professor of chemistry. His current research interest focuses on the fields of sample pretreatment, separation and enrichment materials, solid phase extraction, chromatographic analysis, nucleic acid aptamer, *etc.*



Yifa Chen was born in 1989 in Fujian, China. He received his B.S. degree from School of Chemistry, Beijing Institute of Technology. He subsequently obtained his Ph.D. degree from School of Chemistry and Chemical Engineering, Beijing Institute of Technology under the supervision of Prof. Bo Wang. In 2018, he became an associate professor at Nanjing Normal University (NNU, China). In 2022, he joined South China Normal University (SCNU, China) as a professor of chemistry. His research interest focuses on the fabrication of porous crystalline material based devices like membranes, foams and fibers that can be applicable in energy storage, environment treatment or photo-/electro-catalysis.

Graphical abstract



This review provides a brief introduction on the recent progress of multi-metal porous crystalline materials as advanced electrocatalysts for energy storage and conversion applications.

Declaration of interests

The authors declare that they have no known competing financial interests or personal relationships that could have appeared to influence the work reported in this paper.